Aus dem Deutschen Diabetes-Zentrum
Leibnitz-Zentrum für Diabetes-Forschung
an der Heinrich-Heine-Universität Düsseldorf
Institut für Klinische Biochemie und Pathobiochemie
Direktor: Univ.-Prof. Dr. rer. nat. Hadi Al-Hasani

Effects of nutrition on the expression profile and energy substrate metabolism of diabetes-relevant tissues in a mouse model for skeletal muscle insulin resistance

Dissertation

zur Erlangung des Grades eines Doktors der Medizin

der Medizinischen Fakultät der Heinrich-Heine-Universität Düsseldorf

Vorgelegt von
Jasmin Zadeh (ehem. Eftekharzadeh)
2025

Als Inauguraldissertation gedruckt mit Genehmigung der
Medizinischen Fakultät der Heinrich-Heine-Universität Düsseldorf

gez.:
Dekan: Prof. Dr. med. Nikolaj Klöcker
Erstgutachter/in: Univ.-Prof. Dr. rer. nat. Hadi Al-Hasani
Zweitgutachter/in: Univ.-Prof. Dr. med. Maria Grandoch

Abstract

The RabGTPase-activating proteins (RabGAPs) TBC1D1 and TBC1D4 are key regulators of energy metabolism in skeletal muscle and adipose tissue. Studies on RabGAP-deficient mice have demonstrated impaired insulin- and contraction-stimulated glucose uptake and increased fatty acid utilization in skeletal muscle, resulting in a shift from glucose to lipids as the main fuel source and promoting metabolic flexibility. A loss-of-function mutation in the *TBC1D4* gene has been linked to postprandial hyperglycemia and an elevated risk of type 2 diabetes (T2DM) in a genetically isolated population of Greenlandic Inuits. Over the past few decades, lifestyle changes, such as a reduction in physical activity and the adoption of a Western diet high in carbohydrates and saturated fat, have led to a notable increase in the prevalence of T2DM and cardiovascular disease in these populations.

The objective of this project is to investigate the impact of dietary protein or carbohydrate restriction on the expression profile and energy substrate metabolism in diabetes-relevant organs in RabGAP-deficient mice. Two high-fat diets were employed for this purpose: one high in carbohydrates and low in protein (HCLP) and the other low in carbohydrates and high in protein (LCHP). The impact of the dietary regimens on hepatic insulin sensitivity and on the gene expression of various markers of browning and branched-chain amino acid (BCAA) metabolism in adipose tissue was assessed by Western blot analyses and qPCR, respectively. The investigation revealed that a HCLP diet significantly increased the mRNA expression levels of specific browning markers in subcutaneous white adipose tissue (scWAT) of wildtype (WT) mice, while *Tbc1d4*-knockout (D4KO) mice showed a reduced gene expression of these markers. In contrast, *Tbc1d1*-knockout (D1KO) mice demonstrated decreased gene expression levels of browning markers in scWAT when fed a LCHP diet. In liver tissue, the LCHP diet significantly increased cytosolic phosphoenolpyruvate carboxykinase 1 (PEPCK1) protein abundance in WT, D1KO, and D1/4KO, but not in D4KO mice. In contrast, the protein abundance of glycogen synthase (GS) was significantly reduced in WT mice on the LCHP diet but remained unaltered in RabGAP-deficient mice. On the HCLP diet, D4KO mice exhibited higher GS protein abundance than D1KO and D1/4KO mice. Furthermore, mitochondrial PEPCK2 protein abundance remained unchanged across diets and genotypes.

The results indicate that TBC1D1 and TBC1D4 regulate browning processes in scWAT in a diet-dependent manner. TBC1D4 may enhance mitochondrial activity in scWAT during high-carbohydrate/low-protein feeding, while TBC1D1 may have similar effects during a low-carbohydrate/high-protein diet. Furthermore, the results indicate that *Tbc1d4*-deficiency suppresses hepatic gluconeogenesis during low-carbohydrate/high-protein feeding and promotes glycogen synthesis in D4KO mice on a high-carbohydrate/low-protein diet. Future studies will aim to elucidate the precise molecular mechanisms underlying these genotype-diet interactions.

Zusammenfassung

Die RabGTPase-aktivierenden Proteine (RabGAPs) TBC1D1 und TBC1D4 sind wichtige Regulatoren des Energiestoffwechsels in Skelettmuskulatur und Fettgewebe. Studien an RabGAP-defizienten Mäusen zeigen, dass die Insulin- und kontraktionsstimulierte Glukoseaufnahme beeinträchtigt und die Fettsäurenutzung in der Skelettmuskulatur erhöht ist, was zu einer Verschiebung von Glukose zu Lipiden als Hauptenergiequelle führt und die metabolische Flexibilität fördert. Eine *Loss-of-function*-Mutation im *TBC1D4*-Gen wurde mit postprandialer Hyperglykämie und einem erhöhten Risiko für Typ-2-Diabetes (T2DM) in einer genetisch isolierten Population grönländischer Inuit assoziiert. In den letzten Jahrzehnten haben Lebensstiländerungen, wie reduzierte körperliche Aktivität und eine westliche Ernährung, die Prävalenz von T2DM und Herz-Kreislauf-Erkrankungen in diesen Populationen erhöht.

Ziel dieses Projekts ist es, die Auswirkungen einer Protein- oder Kohlenhydratrestriktion auf das Expressionsprofil und den Energiesubstratstoffwechsel in diabetesrelevanten Organen bei RabGAP-defizienten Mäusen zu untersuchen. Dazu wurden zwei fettreiche Diäten eingesetzt: eine kohlenhydratreiche und proteinarme (HCLP) sowie eine kohlenhydratarme und proteinreiche (LCHP) Diät. Der Einfluss der Diäten auf die hepatische Insulinsensitivität und die Genexpression verschiedener Marker des *Brownings* und des verzweigtkettigen Aminosäurestoffwechsels im subkutanen weißen Fettgewebe (*subcutaneous white adipose tissue*, scWAT) wurden mittels Western Blot-Analysen und qPCR untersucht. Die HCLP-Diät erhöhte die mRNA-Expressionswerte spezifischer *Browning*-Marker im scWAT von Wildtyp (WT)-Mäusen signifikant, während *Tbc1d4*-Knockout (D4KO)-Mäuse eine reduzierte Genexpression dieser Marker aufwiesen. Im Gegensatz dazu zeigten *Tbc1d1*-Knockout (D1KO)-Mäuse bei einer LCHP-Diät verringerte Genexpressionsspiegel von *Browning*-Markern im scWAT. Im Lebergewebe erhöhte die LCHP-Diät die Proteinmenge der cytosolischen Phosphoenolpyruvat-Carboxykinase 1 (PEPCK1) signifikant bei WT-, D1KO- und D1/4KO-, nicht aber bei D4KO-Mäusen. Die Proteinabundanz der Glykogensynthase (GS) war bei WT-Mäusen unter der LCHP-Diät signifikant reduziert, blieb aber bei RabGAP-defizienten Mäusen unverändert. Unter der HCLP-Diät wiesen D4KO-Mäuse eine höhere GS-Proteinmenge auf als D1KO- und D1/4KO-Mäuse. Die Proteinmenge der mitochondrialen PEPCK2 blieb über Diäten und Genotypen hinweg unverändert.

Die Ergebnisse deuten darauf hin, dass TBC1D1 und TBC1D4 *Browning*-Prozesse im scWAT in Abhängigkeit von der Ernährung regulieren. TBC1D4 könnte die mitochondriale Aktivität im scWAT bei einer kohlenhydratreichen/proteinreduzierten Ernährung erhöhen, während TBC1D1 ähnliche Effekte bei einer kohlenhydratarmen/proteinreichen Diät haben könnte. Außerdem deuten die Ergebnisse darauf hin, dass eine *Tbc1d4*-Defizienz die hepatische Gluconeogenese bei einer kohlenhydratarmen/proteinreichen Ernährung unterdrückt und die Glykogensynthese bei einer kohlenhydratreichen/proteinarmen Diät fördert. Zukünftige Studien werden darauf abzielen, die genauen molekularen Mechanismen dieser Genotyp-Diät-Interaktionen aufzuklären.

List of abbreviations

18S	18S ribosomal RNA
AKT	Protein kinase B
AMG4KO	Adipose- and muscle-specific GLUT4–double KO
ANOVA	Analysis of variance
APC	Adipose progenitor cell
APS	Ammonium persulfate
AS160	Akt substrate of 160 kDa
ASC1	Asc-type amino acid transporter 1
ATP	Adenosine triphosphate
B6	C57BL/6J mice
BAT	Brown adipose tissue
BeAT	Beige or brite adipose tissue
BCA	Bicinchoninic acid
BCAA	Branched-chain amino acids
BCAT	Branched-chain amino acid transaminase
BCKA	Branched-chain α-keto acids
BCKDH	Branched-chain α-keto acid dehydrogenase
BCKDHB	Branched-chain α-keto acid dehydrogenase E1 subunit beta
BMP7	Bone morphogenic protein 7
BSA	Bovine serum albumin
bp	base pair
CAR4	Carbonic anhydrase
CD137	Cluster of differentiation 137
cDNA	Complementary DNA
CIDEA	Cell-death inducing DFF45-like effector A
CoA	Coenzyme A
COX8B	Cytochrome c oxidase subunit 8B
Cu^{+} /Cu^{2+}	Copper (I) ions /Copper (II) ions
CVD	cardiovascular disease
D1/4D4KO	*Tbc1d1*/*Tbc1d4*-knockout mice
D1KO	*Tbc1d1*-knockout mice
D4KO	*Tbc1d4*-knockout mice
DBT	Dihydrolipoamide branched-chain transacylase E2
ddH2O	*aqua purificata*
DDZ	Deutsches Diabetes-Zentrum (German Diabetes Center)

dNTP	Deoxynucleotide triphosphates
DNA	Deoxyribonucleic acid
DTT	Dithiothreitol
ECL	Enhanced Chemiluminescence
EDTA	Ethylenediaminetetraacetic acid
EGTA	Ethylene glycol-bis(β-aminoethyl ether)-N,N,N′,N′- tetraacetic acid
EtOH	Ethanol
FGF21	Fibroblast growth factor 21
fwd	forward
GAP	GTPase activating protein
GAPDH	Glyceraldehyde 3-phosphate dehydrogenase
GLUT4	Glucose transporter type 4
GS	Glycogen synthase
GSK3	Glycogen synthase kinase-3
GSV	GLUT4 storage vesicles
HCl	Hydrochloric acid
HCLP	High-carbohydrate low-protein
HFD	High-fat diet
HP	High-protein diet
IgG	Immunoglobulin G
IR	Insulin receptor
IRAP	Insulin-regulated aminopeptidase
IRS	Insulin receptor substrate
kDa	kilodaltons
KO	Knockout
LANUV	Landesamt für Natur, Umwelt und Verbraucherschutz (State Agency for Nature, Environment and Consumer Protection)
LAT	L-amino acid transporter
LCHP	Low-carbohydrate high-protein
LP	Low-protein diet
LSB	Laemmli sample buffer
MetOH	Methanol
MgCl2	Magnesium chloride
Myf-5	Myogenic factor 5
NAFLD	Nonalcoholic fatty liver disease
n	number
NaCl	Sodium chloride

NaHCO3	Sodium hydrogen carbonate
nm	nanometer
o/n	overnight
P2RX5	Purinergic receptor P2X 5
PAGE	Polyacrylamide gel electrophoresis
PCR	Polymerase chain reaction
PDGFRA	Platelet-derived growth factor receptor A
PDH	Pyruvate dehydrogenase
PDHA1	Pyruvate dehydrogenase E1 subunit alpha 1
PDHB	Pyruvate dehydrogenase E1 subunit beta
PDHX	Pyruvate dehydrogenase complex component X
PEPCK	Phosphoenolpyruvate carboxykinase
PI3K	Phosphatidylinositol-3 kinase
PKP	Protein kinase B, =AKT
PPARγ	Peroxisome proliferator-activated receptor-γ
PPARGC1α	Peroxisome proliferator-activated receptor-γ coactivator 1 alpha
PRDM16	PRD1-F1RIZ1 homologous domain containing 16
qPCR	Quantitative real-time polymerase chain reaction
Rab	Ras-related in brain
RabGAP	Rab-GTPase activating protein
RCS	Recombinant congenic strain
rev	reverse
RNA	Ribonucleic acid
Rpm	revolutions per minute
RT	Room temperature
scWAT	subcutaneous white adipose tissue
SD	Standard diet
SDS	Sodium dodecyl sulfate
SEM	Standard error of the mean
Ser	Serine
SERPINA3K	Serine protease inhibitor A3K
SJL	Swiss Jim Lambert mice
SLC2A4	Solute carrier family 2 member 4
SLC23A44	Solute carrier family 23 member 44
SLC43A2	Solute carrier family 43 member 2
SLC7A5	Solute carrier family 7 member 5
SMP	Skimmed milk powder

T2DM	Type 2 diabetes mellitus
TAE	Tris-acetate-EDTA buffer
TBC1D1	TBC1 domain family member 1
TBC1D4	TBC1 domain family member 4
TBE	Transfer buffer
TBS-T	Tris-buffered saline with Tween 20
TBX1	T-box transcription factor 1
TCA	Citric acid cycle
TE	Tris-EDTA buffer
TEMED	Tetramethylethylenediamine
Tris	Tris(hydroxymethyl)aminomethane
UCP1	Uncoupling protein 1
visWAT	Visceral white adipose tissue
WAT	White adipose tissue
WDNM-1-Like	whey acidic protein four-disulfide core domain-21
WT	Wildtype

Table of contents

1 Introduction

1.1 Type 2 diabetes mellitus and obesity

Type 2 diabetes mellitus (T2DM) is a global disease characterized by insulin resistance and high blood glucose levels (Galicia-Garcia et al., 2020). In 2018, more than 500 million cases of T2DM were reported worldwide (KAISER et al., 2018). The prevalence was similar in high- and low-income countries and is expected to increase significantly in the coming years, especially in low-income countries (KAISER et al., 2018).

Heald et al. (2020) showed that T2DM correlates with a reduced life expectancy and life-threatening complications. These complications include macrovascular complications such as cardiovascular disease (CVD), which is the leading cause of death in diabetic patients (Viigimaa et al., 2020), and microvascular complications such as retinopathy, nephropathy, and neuropathy (Gregg et al., 2016). Up to 50% of T2DM patients suffer from neuropathy, which is a major risk factor for amputation. In addition, 25% of T2DM cases have been found to be associated with nephropathy and retinopathy (Faselis et al., 2020).

T2DM is characterized by an imbalance in the metabolism of energy substrates leading to impaired insulin secretion, insulin resistance, or a combination of both (DeFronzo et al., 2015). The onset and progression of T2DM depend on genetic predisposition and various lifestyle factors. An unbalanced diet, characterized by an excess of calories and a lack of physical activity, can lead to the development of obesity and the onset of diabetes (Chatterjee et al., 2017, Ley et al., 2014).

Obesity is a global chronic disease with a current prevalence of more than 650 million adults and is increasing, making it a global epidemic (Boutari and Mantzoros, 2022). Obesity is considered an important risk factor for T2DM by inducing insulin resistance (Kahn et al., 2006). The exact underlying mechanism remains to be determined, but there are several hypotheses about how obesity may promote insulin resistance, including chronic inflammation and lipid overload of the adipose tissue (Chadt et al., 2018).

In addition to T2DM, obesity is also associated with a wide range of other chronic diseases, such as CVD (Piche et al., 2020) and non-alcoholic fatty liver disease (NAFLD) (Romero-Gómez, 2022).

1.2 Insulin-stimulated glucose uptake and RabGAPs

Insulin is an anabolic hormone synthesized and secreted by the beta cells of the pancreas that regulates glucose and lipid metabolism in skeletal muscle, adipose tissue, and the liver (Leney and Tavaré, 2009). Insulin secretion is primarily stimulated by increased postprandial blood glucose levels (Jensen et al., 2008). Insulin activates several signaling cascades by binding to the insulin receptor (IR). This leads to the phosphorylation of the insulin receptor substrates (IRS) 1 and 2. In muscle and adipose tissue, IRS 1

is the predominant substrate activated by insulin, whereas in the liver, IRS 1 and IRS 2 are both major substrates that function in a complementary manner (Thirone et al., 2006). Phosphorylation of IRS 1/2 leads to the activation of the phosphatidylinositol-3-kinase (PI3K) cascade, which in turn causes phosphorylation and thereby activation of protein kinase B (PKB, also known as AKT), a serine/threonine kinase (Manning and Toker, 2017, Sakamoto and Holman, 2008). Insulin-dependent activation of AKT leads to inactivating phosphorylation of the Rab-GTPase-activating proteins (RabGAPs) TBC1 domain family member 4 (TBC1D4, also known as AS160, AKT substrate of 160 kDa) and TBC1 domain family member 1 (TBC1D1) (Sakamoto and Holman, 2008). TBC1D family proteins share the characteristic Rab-GTPase-activating domain, which inactivates the Rab proteins by hydrolyzing GTP to GDP (Mafakheri et al., 2018). Rab proteins belong to a family of approximately 60 small GTPases and are involved in regulating cellular vesicle trafficking, such as glucose transporter type 4 (GLUT4 gene name *SLC2A4*) transport (Leto and Saltiel, 2012). The phosphorylation of TBC1D1 and TBC1D4 disrupts the attachment of RabGAPs to IRAP (Insulin-regulated aminopeptidase), a resident membrane protein of GSV (GLUT4 storage vesicle) (Eickelschulte et al., 2021). This leads to increased translocation of GLUT4 vesicles to the membrane, resulting in increased glucose uptake (Figure 1) (Mafakheri et al., 2018).

TBC1D4 is primarily expressed in the heart, adipose tissue, and oxidative muscle, while TBC1D1 is predominantly expressed in glycolytic skeletal muscle and is nearly absent in adipose tissue (Wang et al., 2013, Chadt et al., 2008). Mutations in *TBC1D1* and *TBC1D4* have been linked to the development of serious metabolic diseases in humans. A coding variant, R125W, was found to be associated with severe familial obesity (Stone et al., 2006), while a premature stop mutation, R363X, in *TBC1D4* leads to extreme postprandial hyperinsulinemia (Dash et al., 2009). Studies on RabGAP-deficient mice have shown impaired insulin-stimulated glucose uptake and enhanced fatty acid utilization, indicating a shift from glucose to lipids as the primary fuel source (Chadt et al., 2008, Dokas et al., 2013, Chadt et al., 2015). Therefore, the two RabGAPs TBC1D1 and TBC1D4 play a crucial role in regulating glucose transport and promoting metabolic flexibility, which allows adaptation and switching of fuel oxidation based on fuel availability (Espelage et al., 2020).

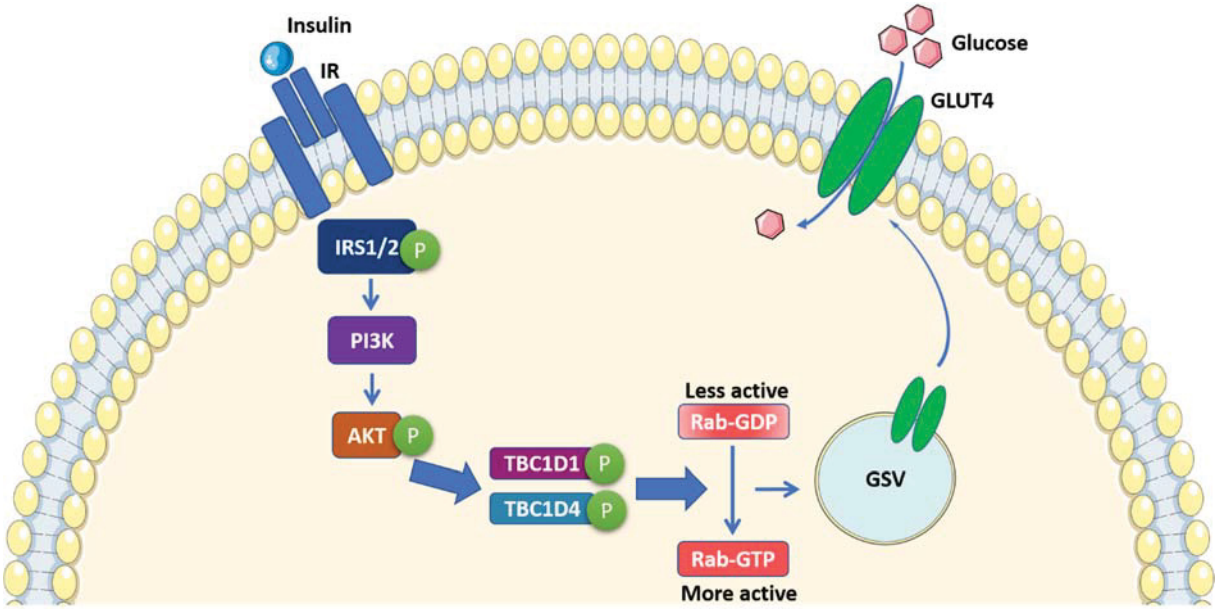

Figure 1: Insulin-stimulated glucose uptake in adipose tissue and skeletal muscle.The insulin-dependent pathway of glucose uptake mediated by GLUT4 translocation involves activation of PI3K and AKT, leading to GLUT4 translocation, which is regulated by the phosphorylation of two RabGAPs, TBC1D1 and TBC1D4. IR = Insulin receptor, IRS = insulin receptor substrate, PI3K = phosphatidylinositol-3-kinase, GSV = GLUT4 storage vesicle (modified from Christian Springer Dissertation (2018) and Sakamoto and Holman (2008)).

1.3 Substrate metabolism in the liver

The liver plays a crucial role in regulating glucose homeostasis, maintaining a normoglycemic state by storing or releasing glucose, depending on the glycemic status (Adeva-Andany et al., 2016).

In contrast to skeletal muscle and adipose tissue, glucose uptake into the liver is not insulin-dependent. The uptake of glucose in hepatocytes is facilitated by hyperglycemia through GLUT2. Insulin inhibits the liver's *de novo* synthesis of glucose (gluconeogenesis), leading to increased glycogen synthesis and glucose storage in the postprandial state to maintain normoglycemia (Sharabi et al., 2015, Hatting et al., 2018). The gluconeogenic pathway enables the metabolism of non-carbohydrate metabolites, such as lactate, glycerol, or amino acids, into glucose. Phosphoenolpyruvate carboxykinase (PEPCK) is a key enzyme that facilitates a rate-limiting step in this pathway and is inhibited by insulin (Yu et al., 2021b, Hatting et al., 2018). PEPCK1 is the cytosolic isoform and the key enzyme for hepatic gluconeogenesis. Meanwhile, mitochondrial PEPCK2 is predominantly expressed in pancreatic beta cells and regulates glucose homeostasis by stimulating insulin release (Yu et al., 2021b).

Additionally, insulin inhibits the enzyme glycogen synthase kinase-3 (GSK3) via phosphorylation, which stimulates hepatic glycogen storage. GSK3 inhibits glycogen synthase (GS), the key enzyme of the glycogen synthesis pathway. Inhibiting GSK3 leads to the phosphorylation of GS and glycogen synthesis, as shown in Figure 2 (Sharabi et al., 2015, Roach et al., 2012). Insulin is a key inhibitor of

gluconeogenesis, therefore, insulin resistance results in decreased glycogen synthesis, increased gluconeogenesis, and hyperglycemia, which leads to diabetic organ damage (Hatting et al., 2018).

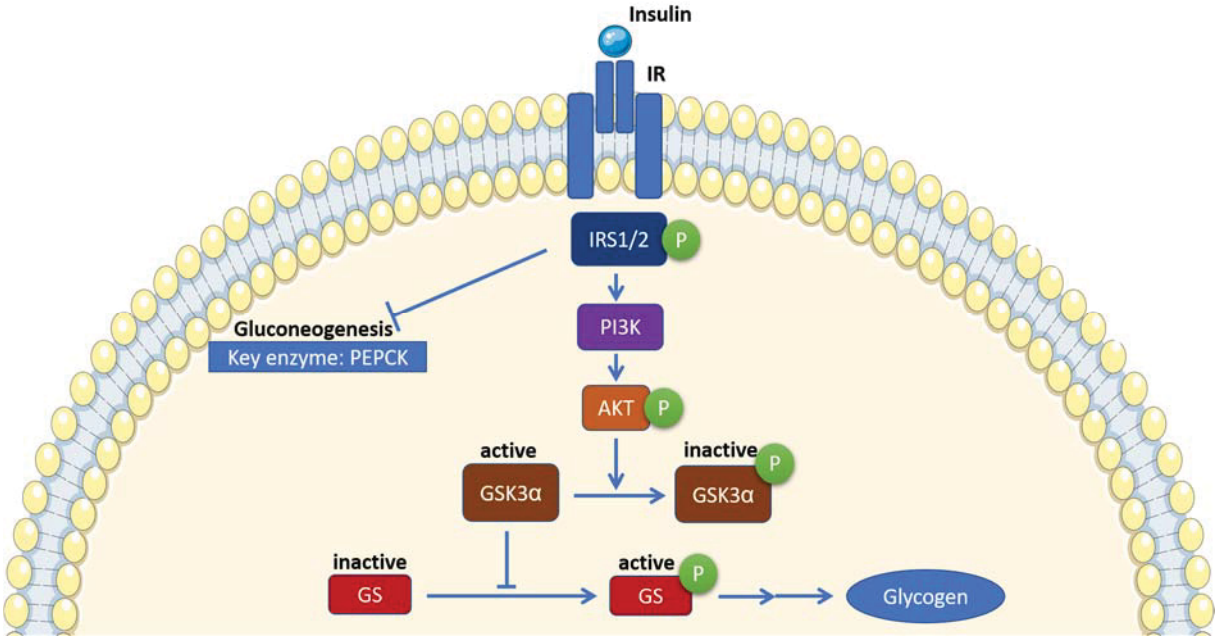

Figure 2: Insulin-regulated glycogen synthesis in the liver. Insulin induces phosphorylation of glycogen synthase kinase-3 (GSK3) by AKT. This inactivates GSK3, which leads to the activation of glycogen synthase (GS) and glycogen synthesis. IR = insulin receptor, IRS1/2 = insulin receptor substrate 1/2, P = phosphorylation.

1.4 Different types of adipose tissue and their functions

Adipose tissue is an endocrine organ and plays a crucial role in maintaining energy homeostasis and metabolic regulation (Murawska-Ciałowicz, 2017, Frigolet and Gutiérrez-Aguilar, 2020). The functions of adipose tissue include energy storage, adipokine secretion, adipogenesis, angiogenesis, extracellular matrix restructuring, steroid metabolism, hemostasis, and body temperature regulation (Tozzi and Novak, 2017, Bays et al., 2008). Different adipose tissue depots can be found in the body, including visceral white adipose tissue (visWAT), which surrounds abdominal organs, and subcutaneous adipose tissue (scWAT), which is mainly located under the skin (Ibrahim, 2010, Mittal, 2019). VisWAT is mostly located in the omental, mesenteric, retroperitoneal, gonadal, and pericardial areas, while scWAT is located abdominally, gluteofemorally, and intramuscularly (Chusyd et al., 2016). According to Frank et al. (2019) and Tatsukawa et al. (2018), 80-90% of the body fat is stored as scWAT. Additionally, a higher accumulation of scWAT in the gluteofemoral region was found to be associated with a lower risk of T2DM when compared to the accumulation of visWAT in the abdominal region (Frank et al., 2019, Tatsukawa et al., 2018).

Adipose tissue can be classified into three types based on its function, coloration, vascularization, and structure: white adipose tissue (WAT), brown adipose tissue (BAT), and beige or brite adipose tissue (BeAT).(Frigolet and Gutiérrez-Aguilar, 2020).

The WAT, which is colored white or yellow, consists of unilocular adipocytes and is less vascularized than BAT, with a low mitochondrial density (Frigolet and Gutiérrez-Aguilar, 2020). In addition to storing energy mainly in the form of triglycerides, it can also secrete regulatory factors known as adipokines (Kershaw and Flier, 2004, Bargut et al., 2017). There are specific WAT markers such as Asc-Type amino acid transporter 1 (*ASC1*), serine protease inhibitor A3K (*SERPINA3K*), and whey acidic protein four-disulfide core domain-21 (*WDNM-1-LIKE*) that are highly expressed in WAT (Garcia et al., 2016). The BAT is composed of multilocular adipocytes that contain several small lipid droplets and is highly vascularized (Bargut et al., 2016). In rodents, the BAT is mainly located in the interscapular, subscapular, axillary, perirenal, and periaortic regions, while in humans it is mostly found in the cervical, supraclavicular, paravertebral, mediastinal, and perirenal regions (Saito et al., 2009, Vernochet et al., 2010). The main function of BAT is non-shivering thermogenesis through uncoupling oxidative phosphorylation in mitochondria and the dissipation of additional energy via uncoupling protein 1 (UCP1) (Bargut et al., 2016, de Jong et al., 2015, Saito et al., 2020). This results in the reentry of protons into the mitochondrial matrix and the generation of heat instead of ATP (Chouchani et al., 2019).

BeAT contains beige or brite (brown in white) adipocytes, which are metabolically intermediate between white and brown adipocytes, with high UCP1 content and a high mitochondrial density. The process by which these adipocytes differentiate from white to brown-like adipocytes is called browning (Frigolet and Gutiérrez-Aguilar, 2020). Browning is induced by various factors, such as cold exposure and β-adrenergic receptor stimulation (Scheel et al., 2022).

Adipose progenitor cells (APCs) can transdifferentiate into white, brown, and beige adipocytes. APCs expressing myogenic factor 5 (Myf-5) transdifferentiate into BAT, whereas WAT progenitor cells have not been shown to express Myf-5. BeAT is derived either directly from APCs of WAT or from transdifferentiation of mature white adipocytes (Wu et al., 2012). Peroxisome proliferator-activated receptor-gamma coactivator 1 alpha (*PPARGC1α*) and PRD1-F1RIZ1 homologous domain containing 16 (*PRDM16*) are crucial for the development of brown adipocytes (Kuryłowicz and Puzianowska-Kuźnicka, 2020, Bargut et al., 2016, Seale et al., 2008). Bone morphogenetic protein 7 (*BMP7*) increases mitochondrial biogenesis, and *PRDM16* is essential for maintaining the beige adipocyte phenotype (Frigolet and Gutiérrez-Aguilar, 2020, Lin et al., 2014, Harms et al., 2014). Some of the BAT markers that are expressed in both brown and beige adipocytes include *PPARGC1α*, cell death activator A (*CIDEA*), cytochrome c oxidase subunit 8 (*COX8*), and *UCP1.* Some genes expressed only in beige adipocytes are cluster of differentiation 137 (*CD137*) and T-box transcription factor (*TBX1*), fibroblast growth factor 21 (*FGF21*), P2X purine receptor 5 (*P2RX5*), and carbonic anhydrase 4 (*CAR4*). Due to the similar characteristics of beige and brown adipocytes, the specific beige adipocyte markers are helpful in classifying the adipocyte types and analyzing the browning process (Garcia et al., 2016, Wu et al., 2012).

1.5 Branched-chain amino acid catabolism

Branched-chain amino acids (BCAA), consisting of leucine, isoleucine, and valine, belong to the group of essential amino acids. Previous studies have demonstrated a strong association between elevated plasma levels of BCAA and obesity, insulin resistance, and T2DM in both humans and rodents (Vanweert et al., 2021, Wang et al., 2011, Lotta et al., 2016). Several studies have investigated the relationship between high BCAA plasma levels and insulin resistance. Lerin et al. (2016), Newgard et al. (2009), Zhou et al. (2019), and White et al. (2016) have shown a causal relationship between the two. However, Mahendran et al. (2017) and Wang et al. (2017) suggest that elevated BCAA levels may be a consequence of insulin resistance. Although the underlying mechanisms of elevated BCAA plasma levels and their association with insulin resistance are still not fully understood, dysfunctional BCAA catabolism may be one of the possible underlying factors (Vanweert et al., 2022). Therefore, BCAA catabolism and clearance, which mainly take place in mitochondria, are crucial.

BCAAs are transported into the cell by the L-amino acid transporter (LAT). The branched-chain amino acid transaminase (BCAT) 1 (cytosolic) or 2 (mitochondrial) converts the BCAAs into branched-chain α-keto acids (BCKAs). The BCKA dehydrogenase complex (BCKDH), which is the key enzyme of the BCAA catabolism, then catalyzes the irreversible decarboxylation of the BCKAs, resulting in the production of acetyl-coenzyme A (CoA) and succinyl-CoA, the end products of the BCAA catabolism. Acetyl-CoA and succinyl-CoA are substrates of the citrate cycle and can be used for ATP synthesis by the mitochondrial respiratory chain or gluconeogenesis (Figure 3) (She et al., 2007, Peng et al., 2020).

Yu et al. (2021a) found that a low-isoleucine diet leads to metabolic reprogramming in the liver and adipose tissue. In the liver, isoleucine has been shown to increase insulin sensitivity. In WAT, isoleucine induces browning by elevating FGF21 expression and increases energy expenditure by activating the FGF21-UCP1 axis. Yoneshiro et al. (2019) showed that cold exposure can lead to the active utilization of BCAA in the mitochondria of BAT for thermogenesis. The transporter Solute Carrier Family 25 Member 44 (SLC25A44), facilitates the transport of BCAA into the mitochondria, thereby playing an important role in BCAA catabolism in BAT. This transporter may serve as a key metabolic regulator for controlling BCAA clearance, according to a study by Yoneshiro et al. (2019). Recent findings by Ma et al. (2022) showed that BCAAs can suppress the browning of WAT by disrupting the interaction between PRDM16 and peroxisome proliferator-activated receptor-γ (PPARγ) due to the acetylation of PRDM16 induced by acetyl-CoA metabolized from BCKAs.

Elevated levels of BCAAs impact the pyruvate dehydrogenase complex (PDH), inhibiting its function and leading to suppressed glucose utilization and impaired metabolic flexibility (Zhang et al., 2014, Lee, 2014, Li et al., 2017). When activated, PDH facilitates the oxidative decarboxylation of pyruvate into acetyl-CoA, which is essential for glucose utilization. Conversely, suppression of PDH leads to the synthesis of acetyl-CoA through fatty acid usage. This highlights the importance of PDH for metabolic

flexibility and the negative impact of high BCAA plasma levels on it (Zhang et al., 2014, Lee, 2014, Li et al., 2017).

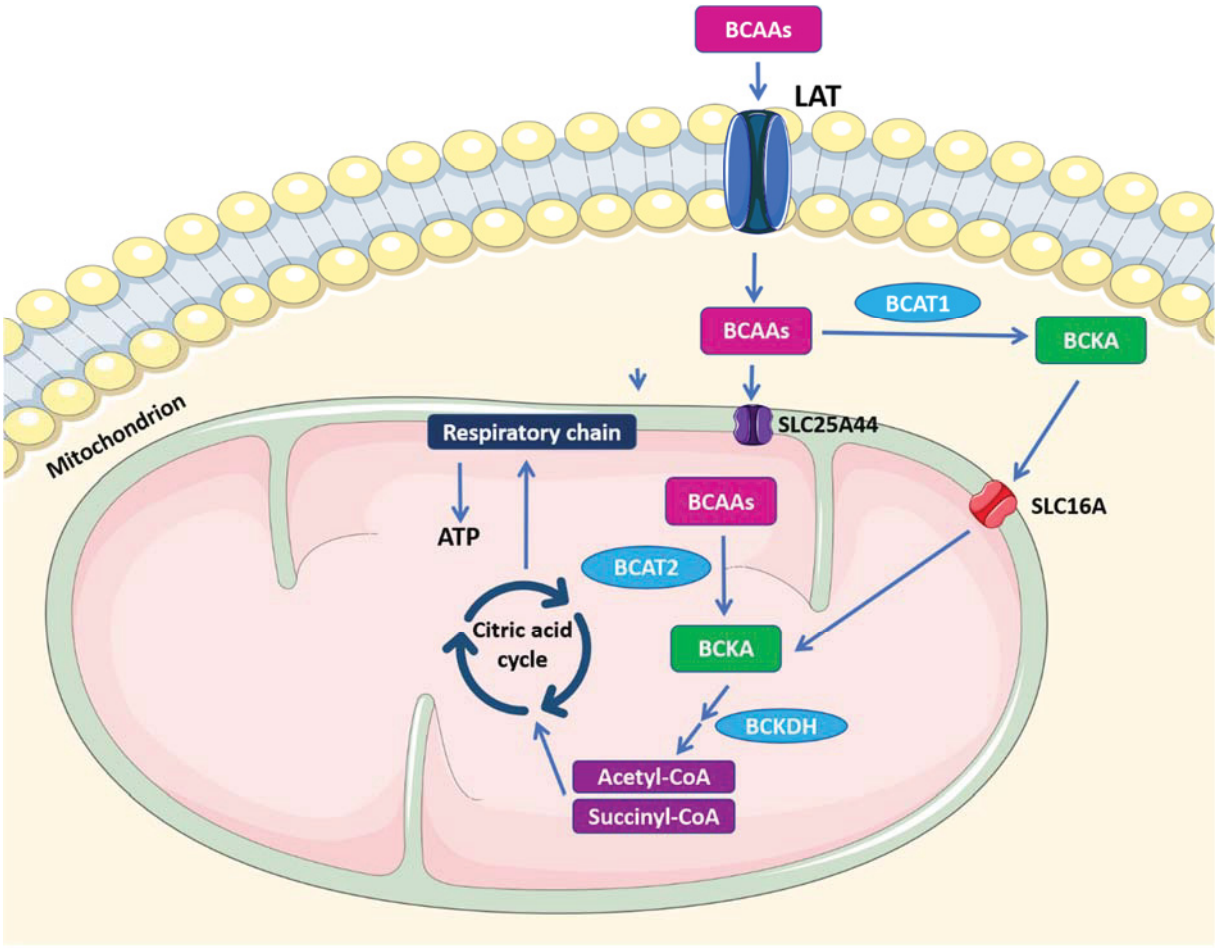

Figure 3: Transport and catabolism of branched-chain amino acids (BCAAs) into adipose tissue. Transport and catabolism of branched-chain amino acids (BCAAs) in the mitochondria of WAT, generating acetyl-CoA and succinyl-CoA, which can be used in the citrate cycle for energy production. LAT = L-amino acid transporter, BCAT1/2 = branched-chain amino acid transaminase, BCKA = branched-chain α-keto acid, SLC25A44 = solute carrier family 25 member 44, SLC16A = solute carrier family 16 (modified from Sebastian Sill, master thesis (2022), Hewton et al. (2021)).

1.6 Impact of nutrition on insulin resistance and energy substrate metabolism

An unbalanced diet can directly affect the body's homeostasis, leading to the development of various metabolic diseases such as CVD and T2DM (Guo et al., 2017). For instance, a high-fat diet (HFD) is frequently used to create a mouse model for obesity, insulin resistance, and T2DM (Nagy and Einwallner, 2018, Zhang et al., 2020). *Tbc1d1*-deficient mice fed a HFD or a standard diet (SD) showed increased fatty acid oxidation, indicating a switched energy substrate preference, higher energy expenditure, and no obesity (Chadt et al., 2015, Dokas et al., 2016, Benninghoff et al., 2020). This demonstrates that the effect of diet also varies with genotype.

Regarding the impact of dietary protein amounts on metabolic health, there are controversies. Previous studies have highlighted the beneficial effects of diets low in protein, especially those low in BCAAs, on metabolic health. These effects include increased insulin sensitivity, increased energy expenditure, and reduced mortality (Levine et al., 2014, Yu et al., 2021a). Conversely, diets with a high protein content have been associated with higher mortality rates, as well as increased CVD and diabetes mellitus (Lagiou et al., 2012, Fontana and Partridge, 2015).

However, Wojcik et al. (2016) found that a high-protein diet with mixed animal and plant sources had beneficial effects on insulin resistance and hepatic steatosis regardless of caloric intake, indicating the importance of the protein source. Research has demonstrated that a diet high in animal protein can intensify insulin resistance, while a diet high in plant-based protein can improve insulin sensitivity. This holds true for both healthy individuals and those with diabetes (Adeva-Andany et al., 2019).

More recently, a loss-of-function mutation in the *TBC1D4* gene has been identified in several Arctic populations. This mutation is associated with postprandial hyperglycemia and an increased risk of T2DM (Manousaki et al., 2016, Moltke et al., 2014, Møller et al., 2021). The traditional diet of Arctic populations was low in carbohydrates but high in protein and fat, particularly in the form of omega-3 fatty acids obtained from sources such as fish (known as the Arctic diet). Until the 1980s, metabolic diseases such as obesity and T2DM had a very low prevalence in Arctic populations. The incidence of T2DM and CVD has increased dramatically in these populations after adopting a Western diet. This diet is characterized by a high-caloric intake consisting of rapidly metabolized carbohydrates, saturated fat, and low dietary protein, accompanied by reduced physical activity (Møller et al., 2021, Munch-Andersen et al., 2012).

1.7 Aim

Prior studies have demonstrated the significance of TBC1D1 and TBC1D4 in regulating glucose transport and metabolic flexibility (Espelage et al., 2020). Moreover, studies on RabGAP-deficient mice have shown impaired insulin-stimulated glucose uptake and enhanced fatty acid oxidation, indicating a shift in energy substrate preference from glucose to lipids as the primary fuel source (Chadt et al., 2015, Benninghoff et al., 2020). Lifestyle changes, such as the switch from a traditional Arctic diet to a Western diet, may be responsible for the dramatic rise in the prevalence of T2DM in several Arctic Inuit populations (Moltke et al., 2014, Møller et al., 2021). Understanding the dietary composition and metabolism of different energy substrates is crucial for comprehending the development of insulin resistance and T2DM.

Therefore, this project aims to investigate the impact of dietary protein or carbohydrate restriction on the expression profile and energy substrate metabolism in diabetes-relevant organs in RabGAP-deficient mice. For this purpose, *Tbc1d1*-knockout (D1KO), *Tbc1d4*-knockout (D4KO), D1/D4KO, and wildtype (WT) mice were fed two different diets prior to this project. Both diets were high-fat diets, with one diet

being high in carbohydrates and low in protein (referred to as the high-carbohydrate low-protein diet or HCLP) and the other diet being low in carbohydrates and high in protein (referred to as the low-carbohydrate high-protein diet or LCHP). The HCLP diet represents a Western diet and the LCHP diet represents an Arctic diet.

This project focuses on two diabetes-relevant organs: the liver and adipose tissue. In the liver, the focus is on elucidating the effect of the HCLP and LCHP diets on the insulin-related glucose metabolism of RabGAP-deficient mice compared to WT mice using Western blot analysis. In the adipose tissue, scWAT was analyzed by quantitative real-time polymerase chain reaction (qPCR) analyses to investigate:

1. The impact of the HCLP and LCHP diets on different browning markers in RabGAP-deficient mice compared to WT mice.
2. The impact of the HCLP and LCHP diets on the BCAA metabolism in RabGAP-deficient mice compared to WT mice.

2 Material and methods

2.1 Materials

2.1.1 Mouse strain

The experiments in this thesis were approved by the State Agency for Nature, Environment and Consumer Protection (LANUV; North Rhine-Westphalia, Germany) (reference number: 81-02.04.2019.A492). All mouse experiments were performed and tissues were collected prior to this work by Anna Scheel (M.Sc.).

Strain	Supplier
C57BL/6J (WT mice)	DDZ, Düsseldorf, Germany
C57BL/6J-*Tbc1d4*$^{-/-}$ (D4KO mice)	DDZ, Düsseldorf, Germany
C57BL/6J-*Tbc1d1*$^{-/-}$ (D1KO mice)	DDZ, Düsseldorf, Germany
RCS.B6.SJL-*Nob1.10*-KO-*Tbc1d4* (D1/4KO mice)	DDZ, Düsseldorf, Germany

Table 1: Mouse strains

2.1.2 Mouse diets

The *Tbc1d1*- and *Tbc1d4*-deficient mice were fed two different high-fat diets, either high in carbohydrates and low in proteins (high-carbohydrate low-protein diet (HCLP)) or *vice versa* (low-carbohydrate high-protein diet (LCHP)) (Research Diets Inc., New Brunswick, NJ, USA). The HCLP diet represents the "Western diet", and the LCHP diet represents the "Arctic diet". All mouse experiments were performed and tissues were collected prior to this work by Anna Scheel (M.Sc.).

Diet	Protein (kcal %)	Carbohydrate (kcal %)	Fat (kcal %)	Total calorie (kcal/g)
High-carbohydrate low-protein diet (HCLP) (#D20092413)	5	40	55	5.1
Low-carbohydrate high-protein diet (LCHP) (#D20092414)	40	5	55	5.1

Table 2: Mouse diets

2.1.3 Devices and materials

Device/Material	Application	Manufacturer
96-well plates	Microtiter plates for BCA assay	Greiner Bio-One, Essen, Germany
Amersham Protran 0.45 µm NC	Nitrocellulose blotting membrane	Cytiva, Washington, D.C., USA
Biometra Eco-Mini	Blotting chamber kit	Analytik-Jena, Jena, Germany
ChemidocTM XRS$^+$ System	Imaging system	Bio-Rad Laboratories, Hercules, CA, USA
Eppendorf Centrifuge 5417 R/ 5424 R	Centrifuge for 1.5 ml and 2.0 ml tubes	Eppendorf, Hamburg, Germany
Eppendorf Mastercycler 5333	cDNA synthesis	Eppendorf, Hamburg, Germany
Eppendorf Thermocycler	PCR analysis	Eppendorf, Hamburg, Germany
Eppendorf Thermomixer comfort	RNA isolation	Eppendorf, Hamburg, Germany
iMark Microplate Absorbance Reader	Microplate reader	Bio-Rad Laboratories, Hercules, CA, USA
MicroAmp Fast Optical 96-Well Reaction Plates (0.1 ml)	Microplates for qPCR analysis	Thermo Fisher Scientific, Waltham, MA, USA
NanoDrop 2000	Measuring DNA concentration	Thermo Fisher Scientific, Waltham, MA, USA
QiaShredder column	RNA isolation	Qiagen, Hilden, Germany
StepOnePlus Real-Time PCR System	qPCR analysis	Thermo Fisher Scientific, Waltham, MA, USA
TissueLyser II	Lysis of muscle samples	Qiagen, Hilden, Germany

Table 3: Devices and materials

2.1.4 Chemicals

Chemicals	Manufacturer
2-propanol	AppliChem, Darmstadt, Germany
Acrylamide 4K Solution (30%) (Mix 37.5:1); A1672	AppliChem, Darmstadt, Germany
Agarose	Biozym Scientific, Oldendorf, Germany
Ammonium persulfate (APS)	Sigma-Aldrich, St. Louis, MO, USA
Bovine serum albumin (BSA) Fraction V (pH 7.0) A1391	AppliChem, Darmstadt, Germany
Bromophenol blue	AppliChem, Darmstadt, Germany
Chloroform	AppliChem, Darmstadt, Germany
Complete - Protease inhibitor cocktail tablets	Roche Diagnostics, Basel, Switzerland
Deoxynucleoside triphosphates (dNTPs)	Roche Diagnostics, Basel, Switzerland
Dithiothreitol (DTT)	AppliChem, Darmstadt, Germany
Ethanol absolute (EtOH)	AppliChem, Darmstadt, Germany
Ethylenediaminetetraacetic acid (EDTA)	Carl Roth, Karlsruhe, Germany
Ethylene glycol-bis (β-aminoethyl ether)-N,N,N′,N′-tetraacetic acid (EGTA)	Carl Roth, Karlsruhe, Germany
Glycerol	AppliChem, Darmstadt, Germany
Glycine	AppliChem, Darmstadt, Germany
HDGreen® Plus DNA Stain	Intas Science Imaging Instruments GmbH, Göttingen, Germany
Hydrochloric acid (HCl) 20%	Carl Roth, Karlsruhe, Germany
Isopropanol	Carl Roth, Karlsruhe, Germany
Magnesiumchlorid ($MgCl_2$)	AppliChem, Darmstadt, Germany
Methanol	Carl Roth, Karlsruhe, Germany
PhosSTOP EASYpack	Roche Diagnostics, Basel, Switzerland
Powdered milk	Carl Roth, Karlsruhe, Germany
2-Propanol	Carl Roth, Karlsruhe, Germany
Proteinase K (≥35 U/mg)	Carl Roth, Karlsruhe, Germany
Random Primer p(dN)6	Roche Diagnostics, Basel, Switzerland
Sodium chloride (NaCl)	Carl Roth, Karlsruhe, Germany
Sodium dodecyl sulfate (SDS) ultrapure	AppliChem, Darmstadt, Germany
Sodium hydrogen carbonate ($NaHCO_3$)	Merck Millipore, Burlington, MA, USA
SYBR Green qPCR primer (gene specific)	Eurogentec, Seraing, Belgium
Tetramethylethylenediamine (TEMED)	Carl Roth, Karlsruhe, Germany

Tris(hydroxymethyl)aminomethane (Tris)	Carl Roth, Karlsruhe, Germany
Triton X-100	Sigma-Aldrich, St. Louis, MO, USA
Tween 20	MP Biomedicals, Irvine, CA, USA
TRIzol	Life Technologies, Carlsbad, CA, USA

Table 4: Chemicals

2.1.5 Buffers and solutions

Solution	Composition/manufacturer
10x Dream Taq Green Buffer	Fermentas GmbH, St. Leon-Rot, Germany
5x Phusion HF Reaction Buffer	Thermo Scientific, Schwerte, Germany
6x DNA loading dye	Fermentas GmbH, St. Leon-Rot, Germany
Blocking solution	5% Powdered milk in TBS-T or 5% BSA in TBS-T
BSA standard (2 mg/ml)	Thermo Fisher Scientific, Waltham, MA, USA
Electrophoresis buffer (1x)	25 mM Tris; 192 mM Glycine; 0.1% (w/v) SDS; ad dH_2O
Laemmli-loading buffer (pH 6.8)	250 mM Tris; 8 wt% SDS; 20 wt% Glycerol; 10 mM EDTA; 6 wt% DTT; 0.2 wt% Bromophenol blue; ad dH_2O
Separating gel buffer (pH 8.8)	1.5 M Tris; 0.4% SDS; ad dH2O
DNA lysis buffer	5 mM EDTA; 0.2 M NaCl; 0.4% SDS; 0.1 M Tris (pH 8.0); ad dH2O
Lysis buffer (Western blot analysis)	150 mM NaCl; 20 mM Tris-HCl; 1 mM EDTA; 1 mM EGTA; 1% Triton X-100; ad dH_2O Added before usage: protease inhibitor (Complete: 40 µl/ml lysis buffer) and phosphatase inhibitor (PhosSTOP: 100 µl/ml lysis buffer)
Resolving gel (12%)	1.56 ml separating gel buffer, 2.4 ml acrylamide (30%), 2.04 ml ddH_2O, 6 mg APS, 6 µl TEMED
Stacking gel	520 µl stacking gel buffer, 260 µl acrylamide (30%), 1.22 ml ddH_2O, 2 mg APS, 2 µl TEMED

TAE buffer (1x)	40 mM Tris, 1 mM EDTA, 57.1 ml acetic acid, pH 8.0
TE buffer (pH 8.0)	10 mM Tris-HCl; 1 mM EDTA; ad dH_2O
1x Transfer buffer (TBE)	25 mM Tris; 192 mM Glycine; 20% Methanol; ad dH_2O
Stacking gel buffer (pH 6.8)	0.5 M Tris; 0.4% SDS; ad dH_2O
1x Washing buffer [Tris-buffered saline with Tween 20 (TBS-T)] (pH 8.0)	10 mM Tris; 150 mM NaCl; 0.05% Tween 20; ad dH_2O

Table 5: Buffers and solutions

2.1.6 Reaction Kits

Reaction Kits	Application	Manufacturer
BCA Protein Assay Kit	Protein content determination	Pierce, Rockford, IL, USA
DreamTaq Green PCR Master Mix	Polymerase-Chain-Reaction (PCR)	Fermentas GmbH, St. Leon-Rot, Germany
GoScript Reverse Transcription System	cDNA synthesis	Promega, Madison, WI, USA
GoTaq qPCR Master Mix	qPCR analysis	Promega, Madison, WI, USA
Western Lightning ECL Pro	Chemiluminescent signal detection in Western blot analyses	Perkin Elmer, Waltham, MA, USA

Table 6: Reaction Kits

2.1.7 Molecular weight size markers

Marker	Manufacturer
PageRuler Prestained Protein Ladder	Thermo Fisher Scientific, Waltham, MA, USA
GeneRuler 100 bp DNA Ladder	Fermentas GmbH, St. Leon-Rot, Germany

Table 7: Molecular weight size marker

2.1.8 Antibodies

Antibodies	Cat.-No., manufacturer
Rabbit-anti-phosphoenolpyruvate carboxykinase (PEPCK) 1	#ab87340, Abcam, Cambridge, UK
Rabbit-anti-PEPCK2	#6924, Cell Signaling Technology, Danvers, MA, USA
Rabbit-anti-glycogen synthase (GS)	#3893, Cell Signaling Technology, Danvers, MA, USA
Rabbit-anti-phospho-GS (Ser641) (pGS)	#3891, Cell Signaling Technology, Danvers, MA, USA
Rabbit-anti- glycogen synthase kinase-3 alpha (GSK3α)	#9338, Cell Signaling Technology, Danvers, MA, USA
Mouse-anti-phospho-GSK3α (Ser21) (pGSK3α)	#9337, Cell Signaling Technology, Danvers, MA, USA
Rabbit-anti-GAPDH (14C10)	#2118, Cell Signaling Technology, Danvers, MA, USA
Mouse IgG	#315-035-008, Jackson ImmunoResearch, West Grove, PA, USA
Rabbit IgG	#111-035-144, Jackson ImmunoResearch, West Grove, PA, USA

Table 8: Antibodies

2.1.9 PCR primers

All PCR primers were synthesized and acquired from Eurogentec (Seraing, Belgium).

Primer	5'-3' sequence
***Tbc1d4* fwd**	AGTAGACTCAGAGTGGTCTTGG
***Tbc1d4* WT rev**	GTCTTCCGACTCCATATTTGC
***Tbc1d4* Geo rev**	GCAGCGCATCGCCTTCTATC
***RCS-B6* fwd**	GGACAAGCAGCTTTCTTGTTT
***RCS-B6* rev**	TCCTGGTCCAGAAGCGAG
***RCS-SJL* fwd**	CAACATTCTGAAGGCCTTCTG
***RCS-SJL* rev**	TCCCTGGCTACAAGCTGAGT

Table 9: PCR-primers

2.1.10 qPCR primers

All primers were acquired from Eurogentec (Seraing, Belgium).

Primer	Exon junction	Fragment size [bp]	5´-3´ sequence
18S	-	268	Forward: ATCATGCAGAACCCACGACA Reverse: GCAAAGGCCCAGAGACTCATT
Bcat1	9 - 10	138	Forward: GAAGGAGATGTTCGGCTCAG Reverse: TCAGTCAGCTTTCCCAGGAT
Bcat2	3 - 4	137	Forward: TGGAGTGGAATAACAAGGCTG Reverse: GTCTCCACCTTTGTATGCTTTC
Bckdhb	2 - 3	146	Forward: AGTCCCTGCAGTATGGGCAAA Reverse: ACCAACAGTGCATCGGAAGA
Bmp7	1 - 2	164	Forward: ACGGACAGGGCTTCTCCTAC Reverse: ATGGTGGTATCGAGGGTGGAA
Cd137	2 - 4	144	Forward: CCTGTGATAACTGTCAGCCTG Reverse: TCTTGAACCTGAAATAGCCTGC
Cidea	5 - UTR	134	Forward: CATACATGCTCCGAGTACTGG Reverse: CATCCCACAGCCTATAACAGAG
Cox8b	1 - 2	145	Forward: AGCCAAAACTCCCACTTCC Reverse: TCTCAGGGATGTGCAACTTC
Dbt	1 - 2	94	Forward: GTGTGCTGGTGGCTATTTCC Rev: ATAGCGAACACAGGTCAGTC
Fgf21	2 - 3	148	Forward: CAAATCCTGGGTGTCAAAGC Reverse: CATGGGCTTCAGACTGGTAC
P2rx5	9 - 11	148	Forward: CAGCTCACCATCCTGTTGTACT Reverse: AGAAAACGTTCTCCCCCTGAG
Pdgfra	12 - 13	143	Forward: GTTGCCTTACGACTCCAGATG Reverse: TCACAGCCACCTTCATTACAG
Pdha1	3 - 5	156	Forward: GTGTGATGGTCAGGAAGCCT Reverse: CAACCTCCTCTTCGTCCTGT
Pdhb	7 - 9	131	Forward: ATTGAAAGGCAAGGGACCCAC Reverse: GGTCTGATGGTGCGCAGATT
Pdhx	3 - 4	108	Forward: GTGAGTGCTGGAGACTCGTT Rev: AGCACCTTCCTCAACCACTAT
Ppargc1α	10 - 11	148	Forward: TCGCTGATGCACTGCCTATG

			Reverse: GAGAGGTCCACAGAGCTGATT
Prdm16	8 - 9	87	Forward: CAGCACGGTGAAGCCATTC Rev: GCGTGCATCCGCTTGTG
Serpina3k	5 - UTR	134	Forward: GCCAAAGTCAATAACCCCAAG Rev: CTTTGCAACAGCCAATCAGAG
Slc7a5	9 -10/UTR	116	Forward: ATGGAGTGTGGCATTGGCTT Rev: ACCGTCACAGAGAAGATAGCC
Slc43a2	4 - 5	162	Forward: GCTGATTGCATATGGAGCAAGTAAC Rev: CGAAGTGAACGTCATGCACAT
Tbx1	1 - 2	145	Forward: TGGGACGAGTTCAATCAGC Reverse: TGTCATCTACGGGCACAAAG
Ucp1	2 - 3	139	Forward: GCATTCAGAGGCAAATCAGC Reverse: GCCACACCTCCAGTCATTAAG
Wdnm-1-like	2 - 3	146	Forward: GCCAGAGGAACAATGTGTCAG Reverse: GTAATCTCCATACATGGCCTCC

Table 10: SYBR Green qPCR primers

2.1.11 Software

Software	Manufacturer
GraphPad Prism 9	GraphPad, San Diego, CA, USA
Image Lab 6.0.1	Bio-Rad Laboratories, Hercules, CA, USA
Microplate Manager Software 6	Bio-Rad Laboratories, Hercules, CA, USA
NanoDrop 2000	Thermo Fisher Scientific, Waltham, MA, USA
StepOne Software v.2.3	Thermo Fisher Scientific, Waltham, MA, USA

Table 11: Software

2.2 Methods

2.2.1 Molecular biological methods

2.2.1.1 Genotyping

2.2.1.1.1 DNA isolation from murine liver and determination of DNA concentration

To verify the different genotypes of the WT, D1KO, D4KO, and D1/4KO mice used in this project, DNA was isolated from the liver tissue. Therefore, 20 µg of liver tissue was weighed and lysed with 200 µl lysis buffer and 10 µl proteinase K (Carl Roth, Karlsruhe, Germany, Table 4) for 2 h at 55°C in a Thermomixer (Eppendorf, Hamburg, Germany). After centrifugation of the samples for 1 min at RT and 9391 x g, the supernatant was transferred to 1.5 ml Safe-Lock tubes, mixed with 200 µl of 2-propanol, and centrifuged for 10 min at RT and 9391 x g. The supernatant was discarded, and 200 µl of 75% ethanol was added. The samples were centrifuged for 5 min at RT and 9391 x g. After removing the supernatant, the tubes containing the DNA pellet were heated for 15 min at 55°C and 135 x g to eliminate any remaining ethanol. The pellets were then resuspended in 100 µl TE buffer (Table 5) and incubated for 5 min at 55°C and 135 x g in a Thermomixer. Subsequently, the DNA concentration was measured at 260 nm using a NanoDrop 2000 device (Thermo Fisher Scientific, Waltham, MA, USA). Thereafter, the isolated DNA was diluted with TE buffer to a concentration of 10 ng/µl and then stored at 4°C until further usage.

2.2.1.1.2 Polymerase chain reaction (PCR)

To amplify a high number of copies of a specific DNA sequence, a polymerase chain reaction (PCR) was performed. This method involves adding a DNA polymerase and complementary primers of the targeted DNA sequence, which synthesizes a new complementary DNA strand in a 5' to 3' direction in repeated cycles under a specific temperature protocol. Each amplification cycle consists of three steps:

1. Denaturation (separation of the double-stranded DNA)
2. Annealing (binding of primers to the single-stranded DNA template)
3. Elongation (synthesis of a complementary DNA strand by DNA polymerase using dNTPs)

To verify the genotype of the experimental animals, two different PCR reactions were used. The first PCR primers were designed to differentiate between *Tbc1d1*-deficient mice and WT mice by targeting the RCS-SJL locus. The second PCR reaction contains included primers targeting the endogenous *Tbc1d4* gene to distinguish between *Tbc1d4*-knockout and wildtype mice. To conduct the PCR, 4 µl of isolated DNA (10 ng/µl) (2.2.1.1.1) were added to 16 µl of a PCR Master Mix (Table 12, Table 14) in Safe-Lock tubes. The mixture was then incubated in a Thermocycler (Eppendorf, Hamburg, Germany) using established PCR protocols (Table 13, Table 15).

***Tbc1d1*-knockout -PCR reagents**	**1x run (a total of 20 µl)**
5x Phusion HF Reaction Buffer	4 µl
dNTPs (2 µl dNTPs + 23 µl ddH_2O)	2 µl
Primer *RCS-B6* fwd	1 µl
Primer *RCS-B6* rev	1 µl
Primer *RCS-SJL* fwd	1 µl
Primer *RCS-SJL* rev	1 µl
ddH_2O	5.8 µl
Phusion High-Fidelity DNA Polymerase	0.2 µl
DNA (10 ng/µl)	4 µl

Table 12: *Tbc1d1*-knockout-PCR master mix

***Tbc1d1*-knockout-PCR program**	**Duration**
Initial denaturation	30 sec 98°C
Denaturation	10 sec 98°C
Annealing	30 sec 65°C
Elongation	5 sec 72°C
Repetition of the four steps above (29x)	
Elongation	7 min 72°C

Table 13: *Tbc1d1*-knockout-PCR program

***Tbc1d4*-knockout-PCR reagents**	**1x run (a total of 20 µl)**
10x Dream Taq Green Buffer	4 µl
dNTPs (2 µl dNTPs + 23 µl ddH_2O)	2 µl
Primer *Tbc1d4* fwd	2 µl
Primer *Tbc1d4* WT rev	1 µl
Primer *Tbc1d4* Geo rev	1 µl
ddH_2O	5.8 µl
Dream Taq Green DNA Polymerase	0.2 µl
DNA (10 ng/µl)	4 µl

Table 14: *Tbc1d4*-knockout-PCR master mix

Tbc1d4-knockout-PCR program	Duration
Initial denaturation	2 min 95°C
Denaturation	30 sec 60°C
Annealing	30 sec 60°C
Elongation	1 min 72°C
Repetition of the four steps above (29x)	
Elongation	5 min 72°C

Table 15: *Tbc1d4*-knockout-PCR program

2.2.1.1.3 Agarose gel electrophoresis

To separate the DNA obtained from PCR (2.2.1.1.2) based on the molecular weight of each fragment, agarose gel electrophoresis is used. Therefore, 1% agarose (Table 4) was added to 1x TAE buffer (Table 5) and boiled at approximately 100°C until the solution became clear. To detect and visualize double-stranded DNA fragments in the gel, 0.1 µg/ml HDGreen® Plus DNA Stain (Table 4) was added to the solution after cooling down to approximately 60°C. This results in the intercalation of HDGreen® Plus DNA Stain in the double-stranded helices of the DNA, which absorbs light in the UV region at a wavelength of 254 nm. PCR samples (20 µl) were loaded into each pocket of the agarose gel in the 1x TAE buffer (Table 5) filled electrophoretic chamber (Compact M, Biometra, Göttingen, Germany). For the *Tbc1d1*-knockout-PCR reaction, 5 µl of 6x DNA Loading dye was added to the 20 µl of PCR samples before loading into the gel. To determine the size of each fragment, a 100 bp ladder (GeneRuler™, Fermentas GmbH, St-Leon-Rot, Germany) was also loaded into one pocket of the gel. The DNA bands were detected using UV light on a ChemiDoc (ChemiDoc XRS+ System, Bio-Rad, München, Germany) after the separation was performed at 100 V. The results were analyzed using Image Lab Software (Image Lab 4.0.1, Bio-Rad, München, Germany).

2.2.1.2 Determination of gene expression

2.2.1.2.1 RNA isolation

To determine the expression levels of genes related to browning and BCAA metabolism in subcutaneous white adipose tissue (scWAT), 100 mg of frozen scWAT was weighed into 2 ml Safe-Lock tubes. 700 µl of TRIzol and a metal bead were added to each tube. The tissue was then homogenized in a TissueLyser II device (Qiagen, Hilden, Germany) for 5 min at 25 Hz and incubated for 3 min at RT. The lysate was then transferred to a QiaShredder column (Qiagen, Hilden, Germany) and centrifuged at 14,000 x g for 2 min at RT. The resulting flow-through was transferred to a new 1.5 ml Safe-Lock tube, and 150 µl of chloroform was added to each sample. The reaction tubes were inverted, incubated for 10 min, and centrifuged at 4°C and 12,000 x g for 15 min. After centrifugation, the solution was separated into three phases: a lower phase (phenol-chloroform phase), an interphase

(DNA-containing), and an upper clear phase containing the RNA. 200 µl of the RNA phase were transferred to a new 1.5 ml Safe-Lock tube. RNA was precipitated by adding 350 µl of 100% isopropanol. The samples were then inverted and incubated for 10 min at RT. After a second centrifugation at 4°C and 12,000 x g for 15 min, the supernatant was discarded. 500 µl of 75% ethanol was added to the obtained RNA-containing pellet. The reaction tubes were vortexed until the pellet detached from the bottom to wash the pellet. After centrifugation at 4°C and 7,500 x g for 5 min, the supernatant was discarded, and the pellet was washed again with 500 µl of 75% ethanol. After carefully decanting the supernatant, the pellet was incubated for 5 min at 55°C in a Thermomixer comfort device (Eppendorf, Hamburg, Germany) and then air-dried for approximately 30 min. The dried pellet was resuspended in 30 µl of RNase-free water, incubated for about 2 min at 400 rpm and 55°C in a Thermomixer comfort device (Eppendorf, Hamburg, Germany), and then stored at -80°C. The concentration of the extracted RNA was measured photometrically at 260 and 280 nm using a Nanodrop 2000 device (Thermo Fisher Scientific, Waltham, MA, USA).

2.2.1.2.2 cDNA synthesis

To synthesize complementary DNA (cDNA) from the isolated RNA (2.2.1.2.1) for the qPCR gene expression analysis (2.2.1.2.3), 1 µg of isolated RNA was mixed with 1 µl of dNTPs and 2 µl of 1:10 diluted hexanucleotide primers on ice. The RNA was filled up to a total volume of 10 µl with nuclease-free water. The samples were incubated at 65 °C for 5 min in the Mastercycler (Eppendorf, Hamburg, Germany) and subsequently for 1 min on ice. This step enables primer annealing by ensuring that the RNA is single-stranded and that the primers anneal to the target efficiently. After centrifuging the samples at 15,871 x g for 1 sec, 7 µl of the reverse transcriptase master mix, containing 4 µl of GoScript 5x reaction buffer, 2 µl of magnesium chloride (25 mM), and 1 µl of GoScript reverse transcriptase was added. The cDNA synthesis was performed in the Mastercycler according to the established protocol shown in Table 16. The synthesized cDNA samples were diluted 1:40 in nuclease-free water and stored at -20°C until qPCR analysis (2.2.1.2.3).

Reaction	Temperature	Duration
Annealing	25°C	5 min
Synthesis	42°C	60 min
Reverse transcriptase inactivation	70°C	15 min
Hold	4°C	

Table 16: Protocol of cDNA synthesis

2.2.1.2.3 Quantitative Real-Time polymerase chain reaction (qRT-PCR)

To measure expression levels of different genes, quantitative real-time polymerase chain reaction (qRT-PCR, qPCR) analyses were used. qRT-PCR analysis quantifies the relative amount of amplified

PCR products by measuring the intercalation of SYBR Green, a fluorescent reporter dye, into the newly synthesized DNA. The fluorescence signal increases in intensity with each cycle and is detectable above a certain threshold (Ct value), which is proportional to the respective gene expression level.

Therefore, 4 µl of cDNA samples diluted at a ratio of 1:40 were added to 5 µl of GoTaq qPCR Master Mix containing SYBR Green dye (Promega, Madison, WI, USA) and 0.5 µl of desired forward and reverse SYBR Green primers in a 1:10 dilution into 96-well plates. The plates were covered with MicroAmp adhesive films (Thermo Fisher Scientific, Waltham, MA, USA) and centrifuged briefly. Afterward, the plates were transferred to a StepOne Plus PCR system (Thermo Fisher Scientific, Waltham, MA, USA), and qPCR analysis was performed using the program outlined in Table 17.

Reaction	Temperature	Duration	Cycles
Hot start	95°C	2 min	1x
Denaturation	95°C	15 sec	40x
Annealing and extension	60°C	60 min	
Dissociation	60-95°C	90 sec	1x

Table 17: qPCR analysis program

The gene expression levels were analyzed with StepOne software v.2.3 (Thermo Fisher Scientific, Waltham, MA, USA) and normalized to the expression levels ($2^{\Delta\Delta ct}$) of the housekeeping gene *18S* (ΔCt) and the mean Ct of WT mice on the HCLP diet.

2.2.2 Biochemical methods

2.2.2.1 Western blot analyses in murine liver tissue

2.2.2.1.1 Preparation of cleared protein lysates

Frozen (-80°C) liver tissue samples from WT, D1KO, D4KO, and D1/D4KO mice fed either a HCLP diet or a LCHP diet, were provided prior to this work by Anna Scheel (M.Sc.). The samples were cut, weighed, and placed in 2 ml Safe-Lock tubes, then stored in liquid nitrogen until further steps were conducted. To determine the protein abundance of selected target proteins, the liver tissue was lysed with 300 µl of lysis buffer per 30 µg of tissue in 2 ml Safe-Lock tubes. After adding metal beads (Qiagen, Hilden, Germany) to each tube, the samples were homogenized using a TissueLyser II (Qiagen, Hilden, Germany) for 5 min at 20 Hz. The samples were incubated for 5 min on ice and centrifuged at 4°C at 15,871 x g for 10 min. The supernatant was transferred to 1.5 ml Safe-Lock tubes, and the protein concentration was determined by a BCA assay (2.2.2.1.2).

2.2.2.1.2 Determination of the protein concentration in cleared protein lysates

To determine the protein concentration of cleared protein lysates, the Bicinchoninic acid (BCA) Protein Assay Kit (Table 6) was used following the manufacturer's instructions. In this colorimetric test, the biuret reaction leads to the reduction of Cu^{2+} ions to Cu^{+} ions in the presence of proteins in alkaline solutions. The reduced Cu^{+} ions then form a chelate complex with BCA, with a measurable absorption maximum at 560 nm. A microtiter plate was pipetted with a BSA standard series with concentrations ranging from 0.025 µg/µl to 0.350 µg/µl, followed by a 1:200 dilution of the samples. Then, 200 µl of a 50:1 mix of reagent A, a carbonate buffer containing BCA reagent, and reagent B, a cupric sulfate solution, were added to each well. The samples were incubated for 30 min at 37°C and measured colorimetrically at 560 nm using an iMark Microplate Absorbance Reader (Bio-Rad Laboratories, Hercules, CA, USA).

2.2.2.1.3 Sodium-dodecyl-sulfate polyacrylamide gel electrophoresis (SDS-PAGE)

To identify specific protein markers, proteins were separated by molecular weight using sodium dodecyl sulfate polyacrylamide gel electrophoresis (SDS-PAGE). A total of 16 µl of protein lysates containing 20 µg of protein, diluted in ddH2O with 1x LSB (Table 5), were prepared. After denaturation at 95°C for 5 min, the samples were briefly centrifuged and loaded onto 12% SDS gels (Table 5) consisting of stacking and resolving gel (Table 5). Eight samples were loaded onto each gel. To determine the exact size of the proteins, a pre-stained marker (Table 7) was loaded into an individual pocket along with the samples. Sodium dodecyl sulfate (SDS) was used to negatively charge the proteins, enabling protein separation according to molecular weight towards the positive pole of an electric field. This method was performed in a chamber filled with electrophoresis buffer (Table 5). Electrophoresis was initiated at 70 V for 15 min until the samples were all aligned in the stacking gel. The voltage was then increased to 150 V for 45-60 min until the proteins were separated, as indicated by the bromophenol blue marker. The gels were subsequently used to transfer the proteins to membranes (2.2.2.1.4).

2.2.2.1.4 Transfer and immobilization of proteins

To transfer and immobilize the separated proteins from the SDS polyacrylamide gels onto a nitrocellulose membrane (Cytiva, Washington, D.C., USA), the gel and membrane were fixated with four Whatman papers and a sponge on each side in a cassette. Each cassette was then placed in a Biometra Eco-Mini blotting chamber (Analytik-Jena, Jena, Germany) filled with transfer buffer (Table 5). Horizontal electrophoresis was used to transfer the previously negatively charged proteins onto the membrane by generating an electric field in the blotting chamber, leading the proteins toward the anode. The transfer was performed at 200 mA for 2 h at 4°C.

2.2.2.1.5 Immunodetection

Following the transfer of the proteins onto the membranes, the membranes were briefly washed with TBS-T (Table 5) and then blocked in 5% BSA/TBS-T for 1 h at RT (Table 5), as described in Table 18, to reduce the unspecific binding of antibodies. Subsequently, the membranes were incubated with the

respective antibodies under the conditions outlined in Table 18. To remove unbound antibodies, the membranes were washed three times with TBS-T for 10 min (or 3 h for GSK-3α). Then, the membranes were incubated with HRP-coupled secondary antibodies diluted in 5% SMP/TBS-T for 1 h at RT (Table 18). Afterward, the membranes were washed again three times with TBS-T for 10 min to remove unbound antibodies. To detect the proteins on the membranes with chemiluminescence (ECL), ECL Pro (Perkin Elmer, Waltham, MA, USA) was used according to the manufacturer's instructions. This resulted in the emission of chemiluminescent light from the antigen-antibody complexes, which were detected by a light-sensitive camera in the ChemiDoc MP imaging system (Bio-Rad Laboratories). Band intensity was quantified using Image Lab 6.0.1 software (Bio-Rad Laboratories), and each band was normalized to the abundance of the housekeeping protein GAPDH on the same membrane.

Protein	**Blocking**	**Antibody** **1st antibody (dilution)** **2nd antibody (dilution)**
PEPCK1	1 h in 5% BSA/TBS-T at RT	o/n at 4°C (1:1,000, 5% BSA in TBS-T)
		1 h at RT (1:20,0000, 5% SMP in TBS-T)
PEPCK2	1 h in 5% BSA/TBS-T at RT	o/n at 4°C (1:1,000, 5% BSA in TBS-T)
		1 h at RT (1:20,0000, 5% SMP in TBS-T)
GS	1 h in 5% BSA/TBS-T at RT	o/n at 4°C (1:1,000, 5% BSA in TBS-T)
		1 h at RT (1:20,0000, 5% SMP in TBS-T)
pGS (Ser^{641})	1 h in 5% BSA/TBS-T at RT	o/n at 4°C (1:1,000, 5% BSA in TBS-T)
		1 h at RT (1:20,0000, 5% SMP in TBS-T)
GSK3α	1 h in 5% BSA/TBS-T at RT	o/n at 4°C (1:1,000, 5% BSA in TBS-T)
		1 h at RT (1:20,0000, 5% SMP in TBS-T)
pGSK3α (Ser^{21})	4 h or o/n in 5% BSA/TBS-T at 4°C	o/n at 4°C (1:1,000, 5% BSA in TBS-T)
		1 h at RT (1:20,0000, 5% SMP in TBS-T)
GAPDH	1 h in 5% BSA/TBS-T at RT	o/n at 4°C (1:2,000, 5% BSA in TBS-T)
		1 h at RT (1:20,0000, 5% SMP in TBS-T)

Table 18: Western Blot analyses conditions for each protein

2.2.3 Statistical analysis

The statistical analyses and figures were visualized using GraphPad Prism 9 software (GraphPad, San Diego, CA, USA). The data presented in this work are presented as mean ± standard error of the

mean (SEM) and the respective number of mice, with the statistical test used in each experiment depicted in the figure legends. The diets and genotypes were compared using a two-way ANOVA with Bonferroni's multiple comparison test. Statistical significance was determined by p-values less than 0.05, and Grubb's test was used to exclude any statistical outliers from further analysis.

3 Results

3.1 Impact of diets with different carbohydrate and protein contents on the glucose metabolism in the liver of RabGAP-deficient mice

3.1.1 Verification of the genotypes of experimental animals

Polymerase chain reaction (PCR) was used to verify the genotype and confirm the homozygosity of the knockout (KO) mice used in this study. Due to the low abundance of RabGAP in the liver, detecting RabGAP-KO through Western blot analysis is challenging. Therefore, PCR of the liver was performed to confirm the genetic makeup of the mice (Szekeres et al., 2012). Two different PCR reactions were conducted (2.2.1.1.2) using liver tissue from the respective mice. The PCR products of wildtype (WT) and *Tbc1d4*-KO (D4KO) mice, which are homozygous for the *Tbc1d1* allele (+/+), displayed a band at the size of approximately 585 bp. In comparison, *Tbc1d1*-KO (D1KO) and D1/D4KO mice with a global knockout for *Tbc1d1* (-/-) displayed a shorter PCR product with a length of approximately 347 bp (Figure 4). Similarly, the PCR products from WT and D1KO mice homozygous for the *Tbc1d4* allele (+/+) showed a band of approximately 350 bp, while D4KO and D1/D4KO mice with a global knockout for *Tbc1d4* (-/-) displayed a shorter PCR product of approximately 250 bp (Figure 5). To verify the experiment's outcome, control samples with predetermined genotypes were used for each gel.

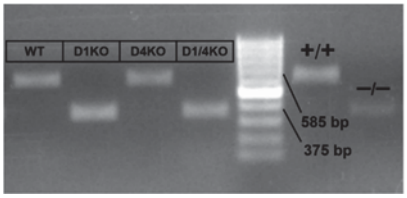

Figure 4: Representative sample of an agarose gel electrophoresis for *Tbc1d1* genotyping. The bands in WT and D4KO mice (+/+) were detected at ~585 bp, in D1KO and D1/4KO mice (-/-) the band was detected at ~347 bp. +/+ = wild type, -/- = *Tbc1d1*-KO control samples.

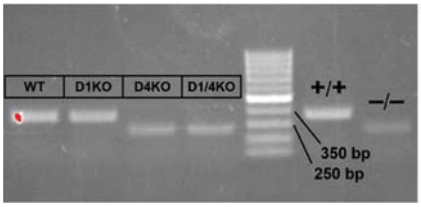

Figure 5: Representative sample of an agarose gel electrophoresis for *Tbc1d4* genotyping. The bands in WT and D1KO mice (+/+) were detected at ~350 bp, in D4KO and D1/4KO mice (-/-) the band was detected at ~250 bp. +/+ = wild type, -/- = *Tbc1d4*-KO control samples.

3.1.2 PEPCK abundance in the liver of RabGAP-deficient mice after LCHP- or HCLP-feeding

To investigate the impact of a dietary protein or carbohydrate restriction on the hepatic glucose homeostasis of RabGAP-deficient mice, the protein abundance of PEPCK1 and PEPCK2, key regulators of the gluconeogenesis pathway, was analyzed by Western blot analysis. The cytosolic isoform PEPCK1 protein abundance was significantly increased in WT (LP: 100 ± 30% vs. HP: 393 ± 57%), D1KO (LP: 125 ± 37% vs. HP: 376 ± 56%), and D1/D4KO mice (LP: 230 ± 43% vs. HP: 478 ± 53%) on LCHP diet compared to mice with the respective genotypes on HCLP diet, whereas D4KO mice (LP: 271 ± 57% vs. HP: 325 ± 53%) exhibited no significant changes on LCHP diet compared to HCLP feeding (Figure 6 A). When comparing the abundance of PEPCK1 in different genotypes on the HCLP diet, an elevated protein abundance was observed in D4KO mice compared to the other genotypes, although the change was not statistically significant (p-value = 0.0565 for WT vs. D4KO). On the LCHP diet, D4KO mice exhibited the lowest overall PEPCK1 protein abundance (Figure 6 A). In contrast, mitochondrial PEPCK2 protein abundance was not affected by either diet or genotype (Figure 6 B).

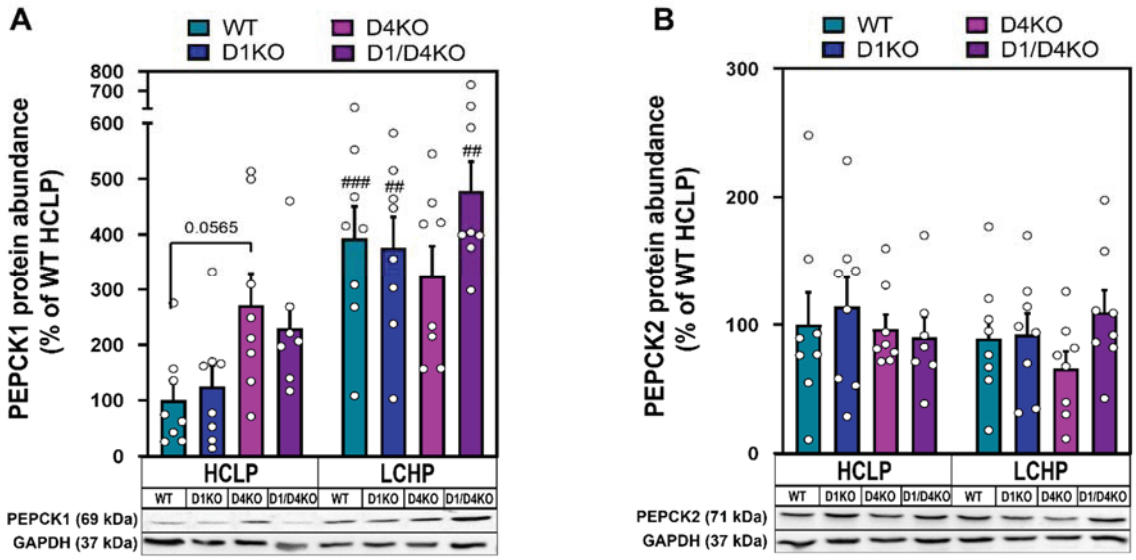

Figure 6: Protein abundance of PEPCK1 and PEPCK2 in the liver of RabGAP-deficient mice fed either a HCLP or a LCHP diet. Representative Western blot analyses and quantification of the protein abundances of PEPCK1 (A) and PEPCK2 (B) in the liver from WT, D1KO, D4KO, and D1/D4KO mice fed a HCLP or LCHP diet, respectively. Protein abundances were normalized to GAPDH and additionally normalized to the mean values of the WT group with a HCLP diet feeding. Data are presented as mean ± SEM (n = 6-8) and were analyzed using two-way ANOVA with Bonferroni's multiple comparisons test. ##, $p < 0.01$; ###, $p < 0.001$ between conditions. HCLP = high-carbohydrate low-protein diet, LCHP = low-carbohydrate high-protein diet.

3.1.3 GS abundance and the phosphorylation state at Ser^{641} in the liver of RabGAP-deficient mice after LCHP- or HCLP-feeding

Glycogen synthase (GS) is a key regulator of hepatic glycogen synthesis and plays an important role in regulating glucose metabolism in the liver. To determine the protein abundance of GS and its phosphorylation at Ser^{641} in the liver of RabGAP-deficient mice fed either a HCLP or a LCHP diet, Western blot analyses were performed. The liver of WT animals on the HCLP diet showed a significantly higher GS protein abundance compared to WT mice on the LCHP diet (LP: 100 ± 26% vs. HP: 29 ± 9%). There were no significant changes in the protein abundance of GS in RabGAP-deficient mice between the HCLP and LCHP diets (Figure 7 A). On HCLP diet, GS protein abundance increased in WT (100 ± 26%) and D4KO mice (97 ± 17%) compared to D1KO (40 ± 10%) and D1/4KO mice (36 ± 11%) (Figure 7 A). The protein content of D4KO mice was higher (92 ± 32%) compared to WT (29 ± 9%), D1KO (50 ± 9%), and D1/D4KO mice (60 ± 16%) on the LCHP diet (Figure 7 A). There were no significant changes in the phosphorylation state of GS at Ser^{641} in response to the diets between the genotypes (Figure 7 B). The ratio of phosphorylated GS at Ser^{641} to the total GS protein content tended to increase on the LCHP diet in WT (LP: 100 ± 26% vs. HP: 225 ± 76%) and D4KO mice (LP: 76 ± 16% vs. HP: 250 ± 114%), but decrease in D1KO (LP: 148 ± 50% vs. HP: 115 ± 32%) and D1/D4KO mice (LP: 155 ± 31% vs. HP: 133 ± 25%) on HCLP diet compared to LCHP diet (Figure **7** C). WT and D4KO mice displayed a lower pGS/GS ratio on the HCLP diet but a higher ratio on the LCHP diet compared to D1KO and D1/D4KO mice (Figure 7 C).

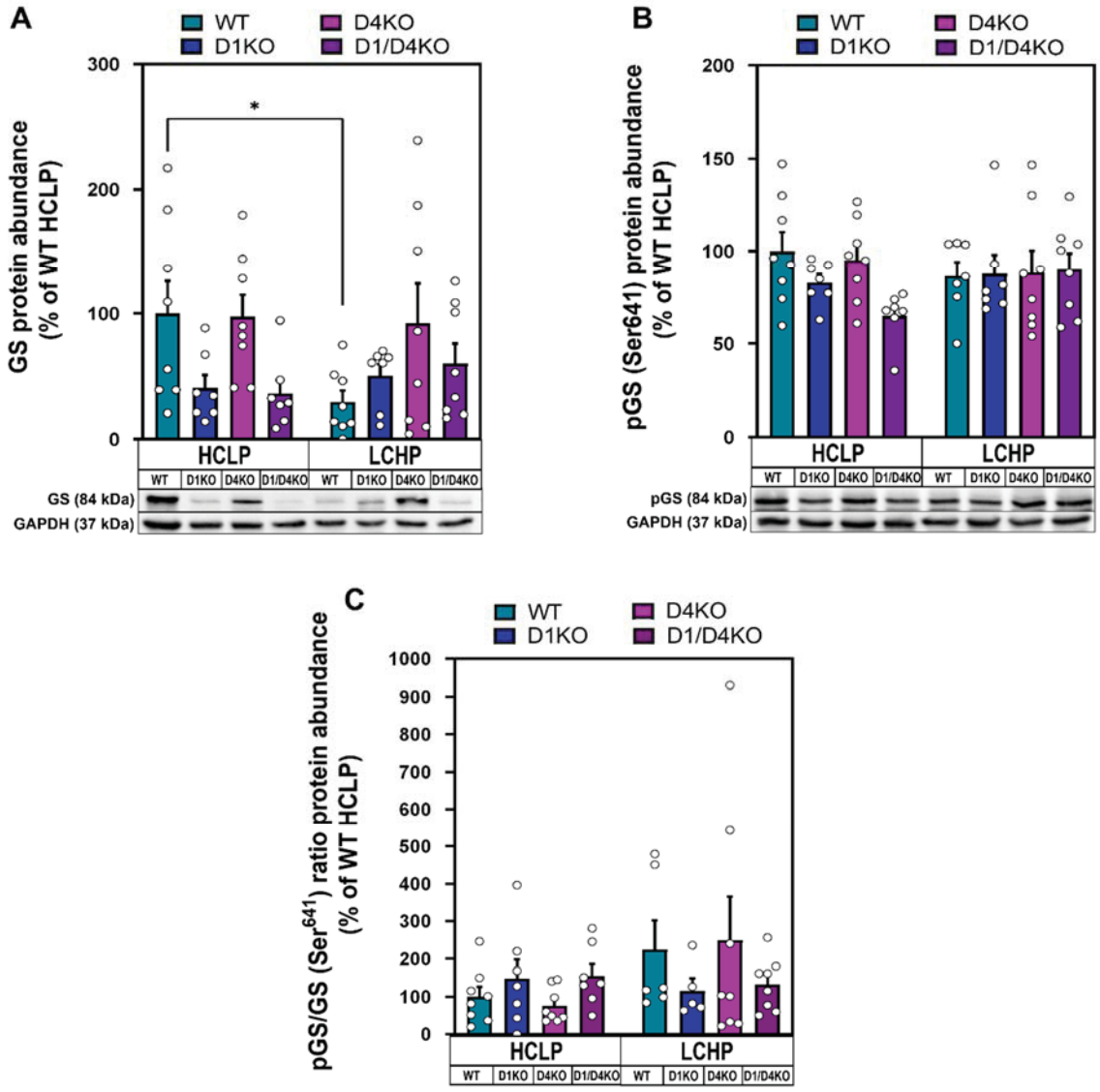

Figure 7: Protein abundance of GS and phosphorylation state of GS at Ser^{641} in the liver of RabGAP-deficient mice fed either a HCLP or a LCHP diet. Representative Western blot analyses and quantification of glycogen synthase (GS) protein abundance (A), GS phosphorylation state at Ser^{641} (B), and the ratio of the phosphorylation state of GS at Ser^{641} to the protein abundance of GS (C) in the liver from WT, D1KO, D4KO, and D1/D4KO mice fed either a HCLP or LCHP diet. The protein abundance and phosphorylation state were normalized to GAPDH and additionally normalized to the mean values of the WT group with HCLP diet feeding. Data are presented as mean ± SEM (n = 5-8) and were analyzed using two-way ANOVA with Bonferroni's multiple comparisons test. #, $p < 0.05$ between conditions. HCLP = high-carbohydrate low-protein diet, LCHP = low-carbohydrate high-protein diet.

3.1.4 GSK3α abundance and phosphorylation state at Ser^{21} in the liver of RabGAP-deficient mice after LCHP- or HCLP-feeding

To investigate the impact of diets with varying carbohydrate and protein contents on the protein abundance and phosphorylation state of glycogen synthase kinase-3 alpha (GSK3α) at Ser^{21} in the liver, Western blot analyses were conducted on the liver of RabGAP-deficient mice fed either a HCLP or

LCHP diet. The results showed that the protein abundance of GSK3α was not significantly affected by carbohydrate restriction or the RabGAP genotype (Figure 8 A). In contrast, the phosphorylation state of GSK3α at Ser^{21} was elevated in WT and RabGAP-deficient mice on the LCHP diet compared to the HCLP diet (Figure 8 B). On the HCLP diet, D1KO (LP: 152 ± 29% vs. HP: 234 ± 70%) and D4KO (LP: 194 ± 56% vs. HP: 260 ± 53%) mice showed increased phosphorylation of GSK3α at Ser^{21} compared to WT (LP: 100 ± 20% vs. HP: 271 ± 45%) and D1/D4KO mice (LP: 124 ± 33% vs. HP: 261 ± 64%). On the LCHP diet, no significant changes were observed between the genotypes (Figure 8 B). The ratio of phosphorylated GSK3α$^{(Ser21)}$ to GSK3α in WT, D4KO, and D1/D4KO mice was not significantly increased on the LCHP diet, whereas the D1KO mice on the LCHP diet were not affected (Figure 8 C).

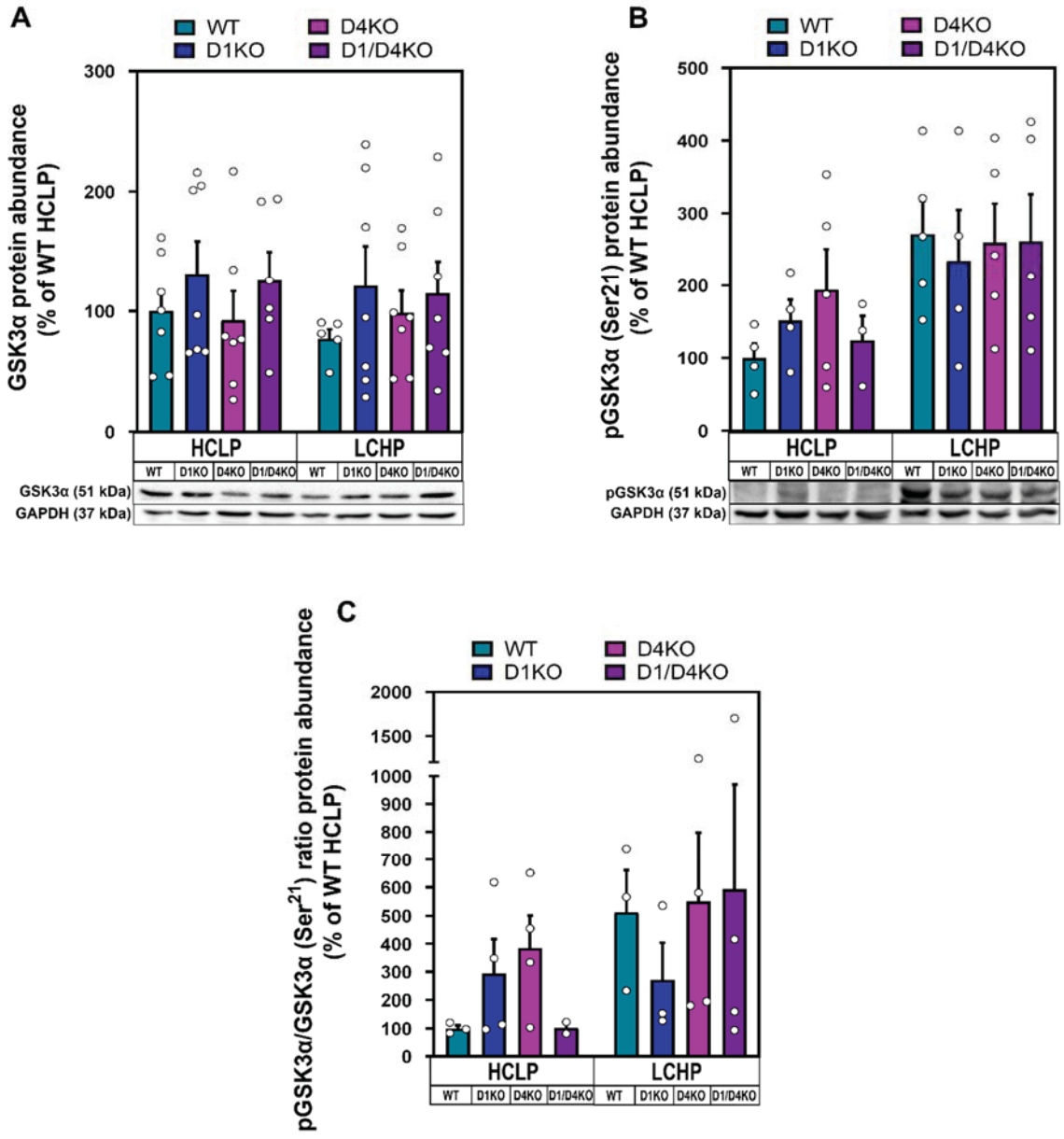

Figure 8: Protein abundance of GSK3α and phosphorylation state of GSK3α at Ser^{21} in the liver of RabGAP-deficient mice fed either a HCLP or a LCHP diet. Representative Western blot analyses and quantification of the protein abundance of glycogen synthase kinase-3 alpha (GSK3α) (A), the phosphorylation state of GSK3α at Ser^{21} (B), and the ratio of the phosphorylation state of GS3α at Ser^{21} to the protein abundance

of GS3α (C) in the liver from WT, D1KO, D4KO, and D1/D4KO mice fed either a HCLP or a LCHP diet. Protein abundances were normalized to GAPDH and additionally normalized to the mean values of the WT group with HCLP diet feeding. Data are presented as mean ± SEM (n = 2-7) and were analyzed using two-way ANOVA with Bonferroni's multiple comparisons test. HCLP = high-carbohydrate low-protein diet, LCHP = low-carbohydrate high-protein diet.

3.2 Impact of diets with different carbohydrate and protein contents on the gene expression profile in adipose tissue of RabGAP-deficient mice

3.2.1 Expression profile of browning markers in scWAT of WT mice after LCHP- or HCLP-feeding

To determine whether the dietary protein-to-carbohydrate ratio affects the browning process in the subcutaneous white adipose tissue (scWAT), gene expression levels of selected browning marker genes in scWAT of WT mice fed either a HCLP or LCHP diet were analyzed using qPCR analyses. The gene expression levels of uncoupling protein 1 (*Ucp1*) (LP: 3.735 ± 1.611 vs. HP: 0.004 ± 0.002), cell death-inducing DFFA-like effector A (*Cidea)* (LP: 1.877 ± 0.680 vs. HP: 0.091 ± 0.031), cytochrome c oxidase subunit 8B (*Cox8b*) (LP: 2.187 ± 0.781 vs. HP: 0.196 ± 0.065), and purinergic receptor P2X 5 (*P2rx5*) (LP: 1.657 ± 0.560 vs. HP: 0.401 ± 0.112) were significantly lower in WT mice fed a LCHP diet compared to those on a HCLP diet (Figure 9). The gene expression levels did not vary between the respective browning markers in HCLP-fed WT mice, however, WT mice on the LCHP diet showed higher gene expression levels of *P2rx5* compared to the other browning markers (Figure 9).

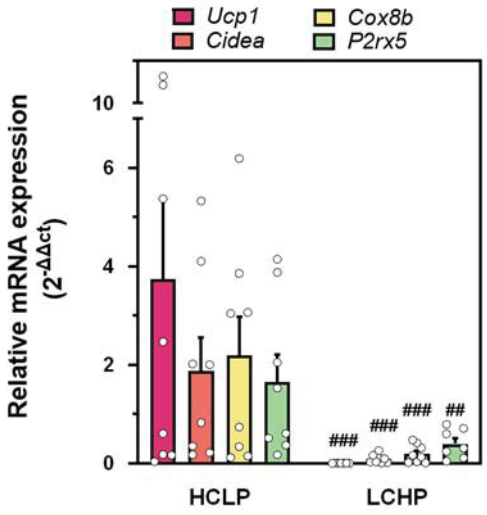

Figure 9: Gene expression levels of browning markers in scWAT of WT mice fed either a HCLP or a LCHP diet. qPCR analyses of the browning marker genes *uncoupling protein 1* (*Ucp1)*, *cell death-inducing DFFA-like effector A* (*Cidea)*, *cytochrome c oxidase subunit 8B* (*Cox8b),* and *purinergic receptor P2X 5 (P2rx5)* in scWAT of WT mice fed either a HCLP or LCHP diet. Gene expression levels were normalized to the housekeeping gene *18S rRNA*. Data are presented as mean ± SEM (n = 8) and were analyzed using two-way ANOVA with

Bonferroni's multiple comparisons test. ##, $p < 0.01$; ###, $p < 0.001$ between indicated groups. HCLP = high-carbohydrate low-protein diet, LCHP = low-carbohydrate high-protein diet.

3.2.2 Expression profile of browning markers in scWAT of RabGAP-deficient mice after LCHP- or HCLP-feeding

Since regular exercise training, cold exposure, and stimulation of the β3-adrenergic receptor can increase the expression levels of browning markers in D4KO mice, it was of interest to investigate the impact of diets with varying dietary carbohydrate and protein on the browning marker gene expression levels in RabGAP-deficient mice. For this purpose, qPCR analyses were performed in scWAT of WT, D1KO, D4KO, and D1/D4KO mice fed either a HCLP or a LCHP diet.

Gene expression levels of peroxisome proliferator-activated receptor gamma coactivator 1 alpha (*Ppargc1α*) were higher in WT (LP: 2.083 ± 0.779 vs. HP: 0.931 ± 0.324), D1KO (LP: 1.095 ± 0.359 vs. HP: 0.256 ± 0.109), and D1/D4KO mice (LP: 0.828 ± 0.384 vs. HP: 0.466 ± 0.195) on the HCLP diet compared to the LCHP diet (Figure 10 A). Additionally, on the HCLP diet, WT mice exhibited higher gene expression levels than RabGAP-deficient mice. On the LCHP diet, D4KO mice (LP: 0.809 ± 0.239 vs. HP: 0.904 ± 0.343) showed lower gene expression levels compared to the other genotypes (Figure 10 A). However, none of these differences were statistically significant.

Gene expression levels of fibroblast growth factor 21 (*Fgf21*) were slightly higher in WT (LP: 1.381 ± 0.515 vs. HP: 1.055 ± 0.266), D1KO (LP: 1.287 ± 0.469 vs. HP: 0.475 ± 0.194), and D1/D4KO mice (LP: 0.433 ± 0.241 vs. HP: 0.194 ± 0.062) on the HCLP diet compared to the LCHP diet. However, *Fgf21* gene expression levels in D4KO mice (LP: 0.660 ± 0.216 vs. HP: 1.827 ± 0.608) on the HCLP diet were lower than on the LCHP diet (Figure 10 B). On the HCLP diet, gene expression levels were lower in D4KO and D1/D4KO mice compared to WT and D1KO mice (Figure 10 B). On the LCHP diet, D4KO mice exhibited higher gene expression levels compared to WT and D1KO animals, and significantly higher levels than D1/4KO mice (Figure 10 B).

The gene expression levels of PRD1-F1RIZ1 homologous domain containing 16 (*Prdm16*) were slightly higher in WT (LP: 1.555 ± 0.455 vs. HP: 1.398 ± 0.513), D1KO (LP: 0.834 ± 0.284 vs. HP: 0.484 ± 0.252), and D1/D4KO mice (LP: 0.849 ± 0.371 vs. HP: 0.623 ± 0.233) on a HCLP diet compared to the LCHP diet, but the difference was not statistically significant. In contrast, *Prdm16* gene expression levels were slightly lower in D4KO mice (LP: 0.589 ± 0.241 vs. HP: 0.864 ± 0.194) on a HCLP diet compared to the LCHP diet (Figure 10 C). On the HCLP diet, WT mice exhibited higher *Prdm16* gene expression levels, whereas D4KO mice showed lower gene expression levels. Furthermore, gene expression levels of WT mice were higher on the LCHP diet compared to D1KO, D4KO, and D1/D4KO mice. Additionally, in comparison to the other genotypes, D1KO mice demonstrated lower gene expression levels (Figure 10 C).

The gene expression levels of platelet-derived growth factor receptor A (*Pdgfra*) were lower in D1KO mice on the LCHP diet compared to the HCLP diet (LP: 1.212 ± 0.447 vs. HP: 0.591 ± 0.211). In

contrast, the gene expression levels were increased in WT (LP: 1.622 ± 0.574 vs. HP: 1.875 ± 0.570) and D4KO mice (LP: 1.094 ± 0.331 vs. HP: 1.614 ± 0.323) (Figure 10 D). Notably, WT mice showed higher gene expression levels compared to RabGAP-deficient mice on the LCHP diet. On the LCHP diet, D1KO mice exhibited lower gene expression levels compared to WT, D4KO, and D1/D4KO mice (Figure 10 D). However, none of the observed differences in Figure 10 D were statistically significant.

Bone morphogenetic protein 7 (*Bmp7*) gene expression levels were higher in D1KO (LP: 0.832 ± 0.370 vs. HP: 3.333 ± 1.353) and D4KO mice (LP: 0.561 ± 0.197 vs. HP: 2.291 ± 0.932) on the LCHP diet compared to the HCLP diet (Figure 10 E). However, in D1/D4KO mice (LP: 6.462 ± 2.508 vs. HP: 3.961 ± 1.587), the gene expression levels were lower on the LCHP diet compared to the HCLP diet (Figure 10 E). On the HCLP diet, *Bmp7* gene expression levels were significantly higher in D1/D4KO mice than in WT, D1KO, and D4KO mice. In comparison, on the LCHP diet, D1KO and D1/D4KO mice showed higher gene expression levels compared to WT and D4KO mice (Figure 10 E).

The gene expression levels of tumor necrosis factor receptor superfamily member 9 (*Tnfrsf9* or cluster of differentiation 137 (*Cd137*)) were slightly higher in D1KO mice (LP: 1.627 ± 0.842 vs. HP: 9.269 ± 4.079) on a LCHP diet compared to the HCLP diet, but the difference was not statistically significant (Figure 10 F). *Cd137* gene expression levels remained unchanged in WT, D4KO, and D1/D4KO mice (Figure 10 F). The gene expression levels were higher in D1/D4KO mice (LP: 10.247 ± 4.327) on the HCLP diet compared to WT (LP: 1.117 ± 0.244, p-value = 0.0953), D1KO (LP: 1.627 ± 0.842), and D4KO mice (LP: 0.972 ± 0.273, p-value = 0.0665). On the LCHP diet, the gene expression levels in D1/D4KO mice (HP: 12.294 ± 3.888) were significantly higher than in WT mice (HP: 0.852 ± 0.287) (Figure 10 F).

The gene expression levels of *P2rx5* showed significantly higher levels in WT mice on the HCLP diet compared to those on the LCHP diet (LP: 1.657 ± 0.560 vs. HP: 0.401 ± 0.112) (Figure 10 G). Additionally, there was an increasing trend in the *P2rx5* gene expression levels in D1KO (LP: 0.861 ± 0.235 vs. HP: 0.345 ± 0.104) and D1/D4KO mice (LP: 0.431 ± 0.212 vs. HP: 0.330 ± 0.080) on the HCLP diet compared to the LCHP diet. However, no changes between the diets were observed in D4KO mice (Figure 10 G). In Figure 10 G, it can be observed that on the HCLP diet, gene expression levels were significantly higher in WT mice compared to D4KO and D1/D4KO mice. However, on the LCHP diet, there were no differences in gene expression levels between the genotypes (Figure 10 G).

The gene expression levels of *Cidea* were significantly higher in WT mice on the HCLP diet compared to LCHP diet (LP: 1.877 ± 0.680 vs. HP: 0.091 ± 0.031) (Figure 10 H). Additionally, the gene expression levels in D1KO (LP: 0.989 ± 0.335 vs. HP: 0.076 ± 0.031), D4KO (LP: 0.204 ± 0.067 vs. HP: 0.032 ± 0.010), and D1/D4KO mice (LP: 0.192 ± 0.067 vs. HP: 0.049 ± 0.015) were also higher on the HCLP diet compared to the LCHP diet (Figure 10 H). Figure 10 H shows that on the HCLP diet gene expression levels were significantly higher in WT mice compared to D4KO and D1/D4KO mice,

whereas on the LCHP diet, gene expression levels were not different between the genotypes (Figure 10 H).

The gene expression levels of *Cox8b* were significantly higher in WT mice on the HCLP diet compared to the LCHP diet (LP: 2.187 ± 0.781 vs. HP: 0.196 ± 0.065) (Figure 10 I). Additionally, it was observed that the expression levels were elevated in D1KO (LP: 1.090 ± 0.420 vs. HP: 0.159 ± 0.057) and D1/D4KO mice (LP: 0.409 ± 0.204 vs. HP: 0.140 ± 0.043) on the HCLP diet in comparison to the LCHP diet. No differences were observed in D4KO mice between the diets (Figure 10 I). On the HCLP diet, WT mice exhibited significantly higher gene expression levels compared to D4KO and D1/D4KO mice (Figure 10 I). However, the gene expression levels showed no alteration between the genotypes on the LCHP diet (Figure 10 I).

The gene expression levels of T-box transcription factor (*TBX1*) exhibited minimal changes between the HCLP and LCHP diets, except for lower gene expression levels in D4KO mice on the HCLP diet compared to the LCHP diet (LP: 0.187 ± 0.045 vs. HP: 0.479 ± 0.136) (Figure 10 J). On both diets, the gene expression levels in D4KO mice were lower than in WT, D1KO, and D1/D4KO mice (Figure 10 J).

Ucp1 gene expression levels were significantly higher in WT mice on a HCLP diet compared to the LCHP diet (LP: 3.735 ± 1.611 vs. HP: 0.004 ± 0.002) (Figure 10 K). Additionally, the gene expression levels of *Ucp1* were increased in D1KO (LP: 1.186 ± 0.500 vs. HP: 0.002 ± 0.001) and D1/D4KO mice (LP: 0.117 ± 0.054 vs. HP: 0.001 ± 0.001) on a HCLP diet in comparison to a LCHP diet. However, there were no changes in *Ucp1* gene expression levels in *D4KO* mice between the diets (Figure 10 K). On the HCLP diet, WT mice exhibited significantly higher gene expression levels compared to D1KO, D4KO, and D1/D4KO mice. In contrast, gene expression levels remained unchanged across all genotypes on the LCHP diet (Figure 10 K).

The gene expression levels of the browning markers *Pargc1a*, *Fgf21*, *Prdm16*, and *Pdgfra* (Figure 10 A, B, C, D) were lower in D1KO mice on the LCHP diet, while *Bmp7 and Cd137* gene expression levels (Figure 10 E, F) were increased in D1KO mice on the same diet. Additionally, the gene expression levels of *P2rx5, Cidea*, *Cox8b*, *Tbx1*, and *Ucp1* (Figure 10 G, H, I, J, K) were lower in D4KO mice on the HCLP diet compared to WT, D1KO, and D1/D4KO mice.

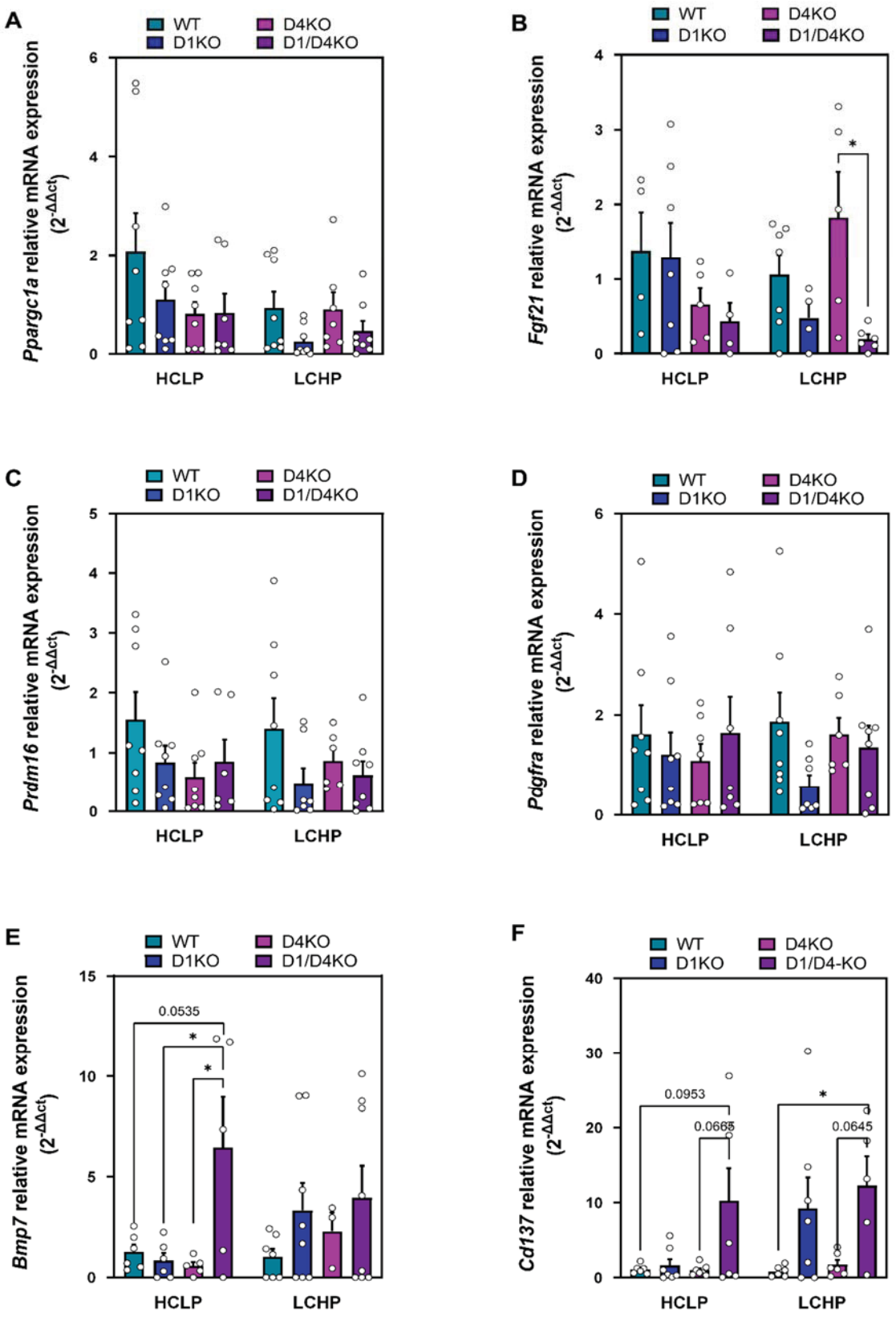
A
WT
D1KO
D4KO
D1/D4KO
Ppargc1a relative mRNA expression
(2-ΔΔct)
HCLP
LCHP
B
Fgf21 relative mRNA expression
(2-ΔΔct)
*
C
Prdm16 relative mRNA expression
(2-ΔΔct)
D
Pdgfra relative mRNA expression
(2-ΔΔct)
E
Bmp7 relative mRNA expression
(2-ΔΔct)
0.0535
F
D1/D4-KO
Cd137 relative mRNA expression
(2-ΔΔct)
0.0953
0.0665
0.0645

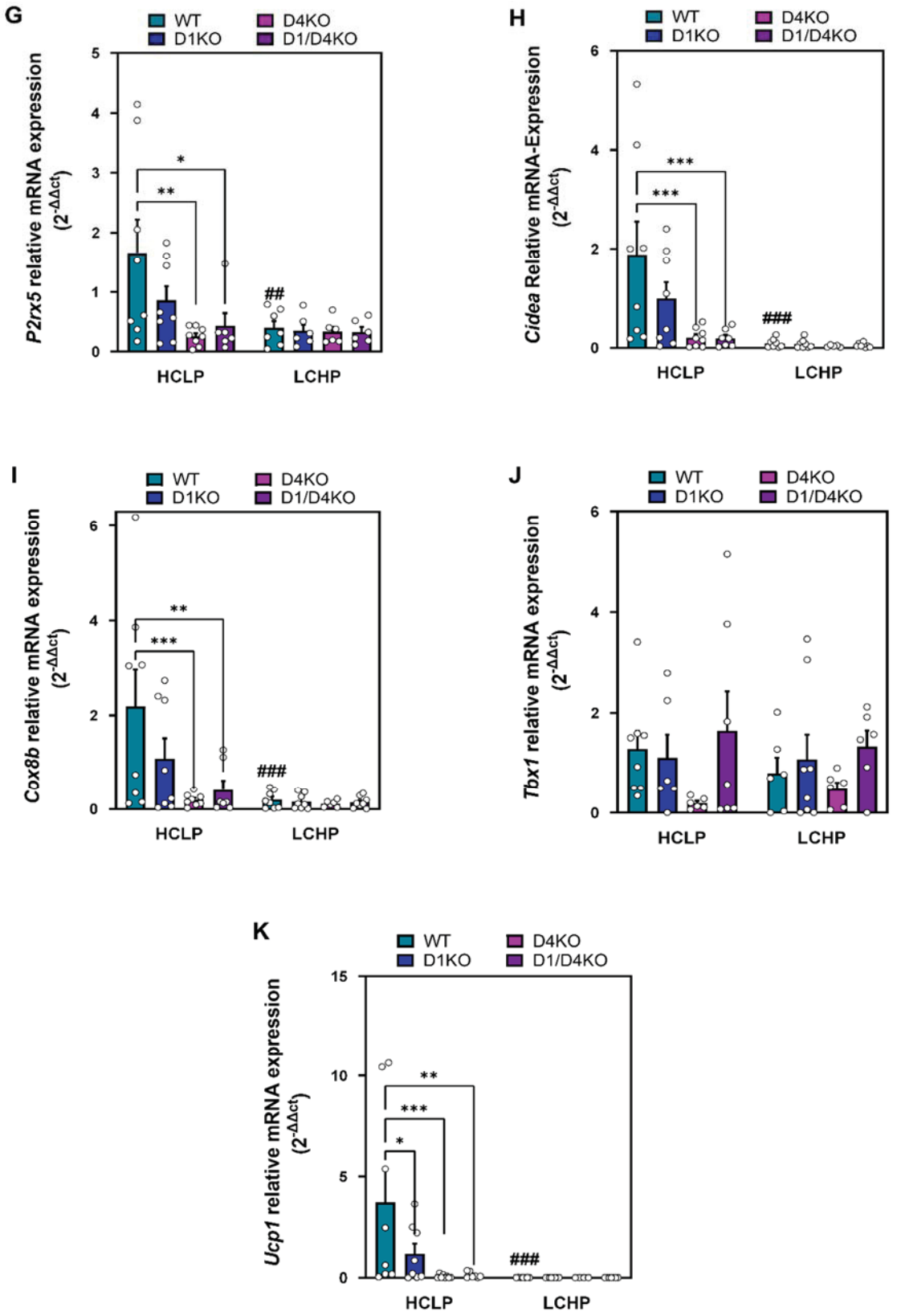

Figure 10: Gene expression levels of browning markers in scWAT of RabGAP-deficient mice fed a HCLP or LCHP diet. qPCR analysis of the browning markers peroxisome proliferator-activated receptor gamma coactivator 1 alpha (*Ppargc1α*) (A), fibroblast growth factor 21 (*Fgf21*) (B), PRD1-F1RIZ1 homologous domain containing 16 (*Prdm16*) (C), platelet-derived growth factor receptor A (*Pdgfra*) (D), bone morphogenetic protein 7 (*Bmp7*) (E), *Cd137* (F), *P2rx5* (G), *Cidea* (H), *Cox8b* (I), T-box transcription factor 1 (*Tbx1*) (J) and *Ucp1* (K) in WT, D1KO, D4KO and D1/D4KO mice fed either a HCLP or a LCHP diet. Gene expression levels were normalized to the housekeeping gene *18S rRNA*. Data are presented as mean ± SEM (n = 3-8) and were analyzed

using two-way ANOVA with Bonferroni's multiple comparisons test. *, $p < 0.05$; **, $p < 0.01$, *** and $p < 0.001$, between indicated groups and ##, $p < 0.01$; ###, $p < 0.001$ between conditions. HCLP = high-carbohydrate low-protein diet, LCHP = low-carbohydrate high-protein diet.

3.2.3 Expression profile of WAT markers in scWAT of RabGAP-deficient mice after LCHP- or HCLP-feeding

After investigating the gene expression levels of various browning markers, it was also of interest to elucidate the effects of a dietary protein or carbohydrate restriction on gene expression levels of white adipose tissue (WAT) markers in scWAT of RabGAP-deficient mice fed either a HCLP or LCHP diet. Therefore, qPCR analyses were performed.

The gene expression levels of whey acidic protein four-disulfide core domain-21 (*Wdnm1like*) were significantly increased in WT mice on the LCHP diet compared to the HCLP diet (LP: 1.281 ± 0.255 vs. HP: 2.944 ± 0.655) Figure 11 A). Furthermore, the gene expression levels increased in D4KO mice (LP: 1.832 ± 0.457 vs. HP: 2.675 ± 0.686), whereas they decreased in D1KO (LP: 1.079 ± 0.375 vs. HP: 0.548 ± 0.147) and D1/D4KO mice (LP: 1.010 ± 0.335 vs. HP: 0.691 ± 0.189) when fed a LCHP diet compared to a HCLP diet. However, these changes were not statistically significant (Figure 11 A). Compared to D1KO and D1/D4KO mice, WT and D4KO mice showed slightly elevated gene expression levels on the HCLP diet. However, on the LCHP diet, both WT and D4KO mice exhibited significantly increased gene expression levels compared to D1KO and D1/D4KO mice (Figure 11 A).

The gene expression levels of the WAT marker serine protease inhibitor A3K (*Serpina3k*) were also higher in WT (LP: 1.162 ± 0.286 vs. HP: 2.764 ± 0.863), D1KO (LP: 1.689 ± 0.577 vs. HP: 2.787 ± 0.359), and D1/D4KO mice (LP: 1.524 ± 0.407 vs. HP: 2.097 ± 0.227) on LCHP diet compared to HCLP diet (Figure 11 B). In contrast, the gene expression levels were not altered in D4KO mice between both diets (Figure 11 B). On the HCLP diet, gene expression levels in RabGAP-deficient mice were higher than in WT mice. On the LCHP diet, gene expression levels in WT and D1KO mice were higher compared to D4KO and D1/D4KO mice (Figure 11 B).

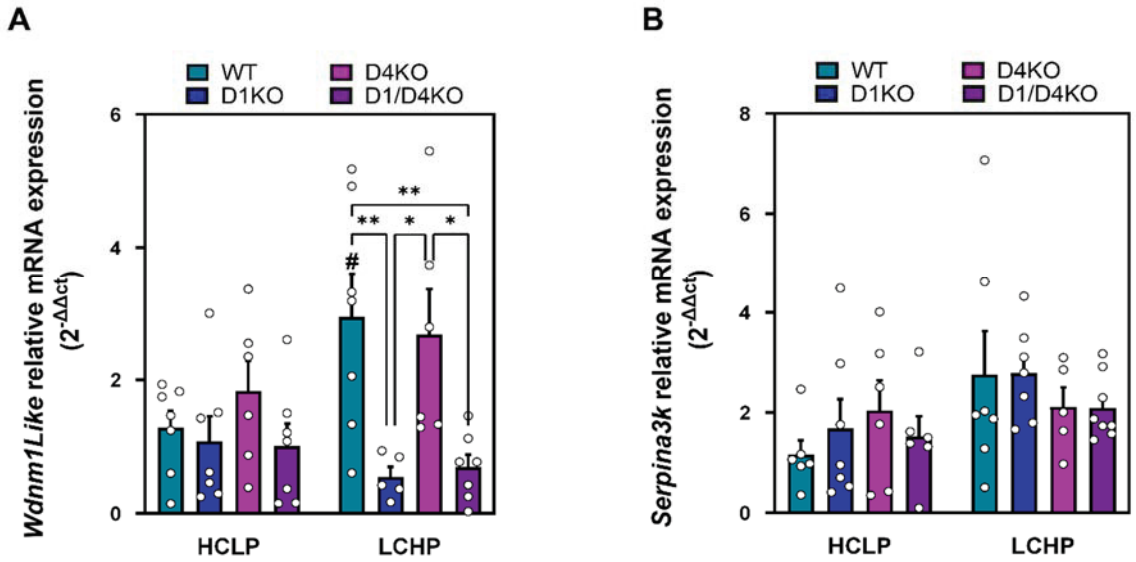

Figure 11: Gene expression levels of WAT markers in scWAT of RabGAP-deficient mice fed a HCLP or LCHP diet. qPCR analysis of the WAT markers whey acidic protein four-disulfide core domain-21 (*Wdnm1-like)* (A) serine protease inhibitor A3K (*Serpina3k*) (B) in WT, D1KO, D4KO and D1/D4KO mice fed either a HCLP or a LCHP diet. Gene expression levels were normalized to the housekeeping gene *18S rRNA*. Data are presented as mean ± SEM (n = 5-8) and were analyzed using two-way ANOVA with Bonferroni's multiple comparisons test. *, $p < 0.05$; **, $p < 0.01$ between indicated groups and #, $p < 0.05$ between conditions. HCLP = high-carbohydrate low-protein diet, LCHP = low-carbohydrate high-protein diet.

3.2.4 Expression profile of *Slc2a4* in scWAT of RabGAP- deficient mice after LCHP- or HCLP-feeding

Since GLUT4 plays a crucial role in mediating glucose uptake, it was of interest to investigate the impact of different diets on the gene expression levels of the GLUT4 gene solute carrier family 2 (facilitated glucose transporter) member 4 (*Slc2a4*) in scWAT of RabGAP-deficient mice on either a HCLP or a LCHP diet. The qPCR analysis revealed lower *Slc2a4* gene expression levels in WT (LP: 2.801 ± 1.172 vs. HP: 1.162 ± 0.447), D1KO (LP: 0.836 ± 0.301 vs. HP: 0.415 ± 0.228), and D1/D4KO mice (LP: 1.456 ± 0.795 vs. HP: 0.367 ± 0.104) on the LCHP diet compared to the HCLP diet. In contrast, there were nearly no changes in the gene expression levels in D4KO mice (Figure 12). Furthermore, the analysis showed higher gene expression levels in WT mice compared to RabGAP-deficient mice in both diets. On the HCLP diet, *Slc2a4* gene expression levels were lower in D4KO mice than in WT, D1KO, and D1/D4KO mice, and in particular significantly lower than the gene expression levels in WT mice (Figure 12).

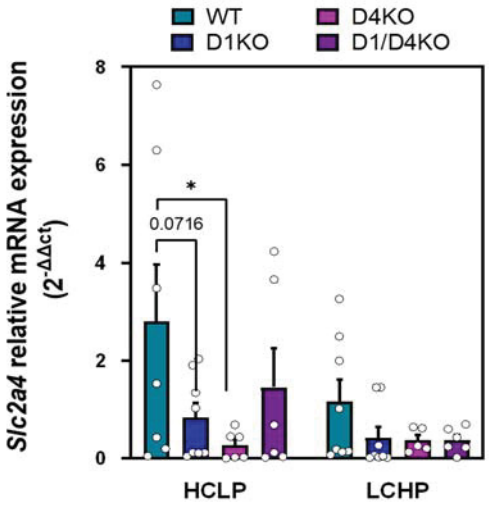

Figure 12: Gene expression levels of *Slc2a4* in scWAT of RabGAP-deficient mice fed a HCLP or LCHP diet. qPCR analysis of the gene expression levels of solute carrier family 2 (facilitated glucose transporter) member 4 (*Slc2a4*), in WT, D1KO, D4KO and D1/D4KO mice fed either a HCLP or a LCHP diet. Gene expression levels were normalized to the housekeeping gene *18S rRNA*. Data are presented as mean ± SEM (n = 5-8) and were analyzed using two-way ANOVA with Bonferroni's multiple comparisons test. *, $p < 0.05$ between indicated groups. HCLP = high-carbohydrate low-protein diet, LCHP = low-carbohydrate high-protein diet.

3.2.5 Expression profile of BCAA metabolism-related genes in RabGAP-deficient mice after LCHP- or HCLP-feeding

Since the LCHP diet contains higher amounts of branched-chain amino acids (BCAA) compared to the HCLP diet, it was of interest to investigate the impact of HCLP and LCHP diets on the gene expression levels of several BCAA metabolism-related genes.

The gene expression levels of the mitochondrial enzyme branched-chain amino acid transaminase 1 (*Bcat1*) increased in D1/D4KO (LP: 3.622 ± 1.645 vs. HP: 1.258 ± 0.268) and D4KO mice (LP: 1.773 ± 0.527 vs. HP: 1.315 ± 0.338) on the HCLP diet compared to the LCHP diet, while no changes were observed in WT and D1KO mice between the diets (Figure 13 A). Additionally, D1/D4KO mice on the HCLP diet, showed higher gene expression levels compared to the WT, D1KO, and D1/D4KO mice, although this difference was not statistically significant. On the LCHP diet, there were no significant differences in gene expression levels between WT and RabGAP-deficient mice (Figure 13 A).

The gene expression levels of the cytosolic isoform branched-chain amino acid transaminase 2 (*Bcat2*) increased in WT (LP: 0.934 ± 0.449 vs. HP: 2.421 ± 0.895) and D4KO mice (LP: 0.507 ± 0.193 vs. HP: 0.909 ± 0.339) on the LCHP diet compared to the HCLP diet, while decreasing in D1KO (LP: 1.490 ± 0.570 vs. HP: 1.035 ± 0.511) and D1/D4KO mice (LP: 2.364 ± 1.302 vs. HP: 0.833 ± 0.292) (Figure 13 B). On the HCLP diet, D1KO and D1/D4KO mice exhibited higher gene expression levels compared to WT and D4KO mice, whereas on the LCHP diet, WT mice showed higher gene expression levels compared to RabGAP-deficient mice (Figure 13 B).

The gene expression levels of the E1 subunit beta of the branched-chain keto acid dehydrogenase (*Bckdhb*), were higher on the HCLP diet compared to the LCHP diet (Figure 13 C). Specifically, WT mice showed significantly higher gene expression levels on the HCLP diet (LP: 2.295 ± 0.775 vs. HP: 0.788 ± 0.251, p-value = 0.04) (Figure 13 C). On the HCLP diet, WT mice showed higher gene expression levels than RabGAP-deficient mice (p-value = 0.08), whereas, on the LCHP diet, there were no changes in gene expression levels between the genotypes (Figure 13 C).

The gene expression levels of dihydrolipoamide branched-chain transacylase E2 (*Dbt*), another subunit of the enzyme branched-chain alpha-ketoacid dehydrogenase (BCKDH), were lower in D1KO (LP: 1.403 ± 0.499 vs. HP: 0.626 ± 0.278), D4KO (LP: 0.747 ± 0.257 vs. HP: 0.874 ± 0.311), and D1/D4KO mice (LP: 1.726 ± 0.908 vs. HP: 0.394 ± 0.112) on the LCHP diet compared to the HCLP diet. *Dbt* gene expression levels were unaltered in WT mice in response to protein restriction (Figure 13 D). On the HCLP diet, D4KO mice exhibited lower gene expression levels compared to WT, D1KO, and D1/D4KO mice. Meanwhile, on the LCHP diet, *Dbt* gene expression levels in WT mice were higher than in RabGAP-deficient mice (Figure 13 D).

Amino acid transporter solute carrier family 43 member 2 (*Slc43a2*) gene expression levels were higher in D1KO mice (LP: 0.262 ± 0.130 vs. HP: 2.423 ± 1.217) and lower in D1/D4KO mice (LP: 4.515 ± 2.567 vs. HP: 2.664 ± 1.303) on the LCHP diet compared to the HCLP diet (Figure 13 E). *Slc43a2* gene expression levels in WT and D4KO mice were unaltered between the diets (Figure 13 E). On the HCLP diet, D1/D4KO mice exhibited higher gene expression levels compared to WT, D1KO, and D4KO mice, while on the LCHP diet, D1KO and D1/D4KO mice showed higher gene expression levels compared to WT and D4KO mice (Figure 13 E).

The gene expression levels of the amino acid transporter, solute carrier family 7 member 5 (*Slc7a5*), showed higher levels on the LCHP diet compared to the HCLP diet in D1KO mice (LP: 1.800 ± 0.702 vs. HP: 9.638 ± 4.266), a decreasing trend in D1/D4KO mice (LP: 10.287 ± 4.723 vs. HP: 7.832 ± 3.874), and no changes in WT and D4KO mice (Figure 13 F). On the HCLP diet, *Slc7a5* gene expression levels in D1/D4KO mice were higher than in WT, D1KO, and D4KO mice (p-value = 0.0923). Meanwhile, on the LCHP diet, D1KO and D1/D4KO mice showed increased gene expression levels compared to WT and D4KO mice (Figure 13 F).

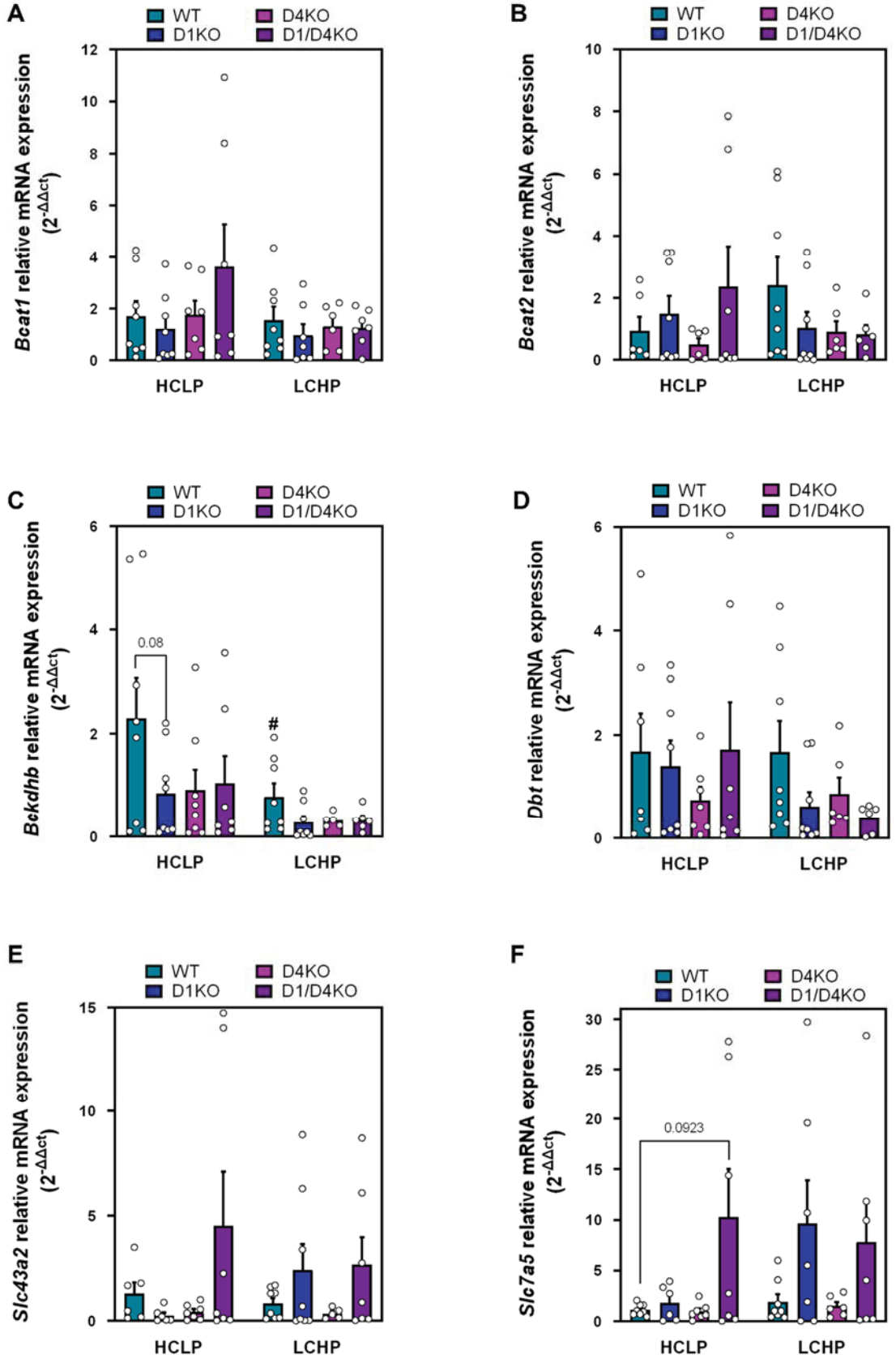

Figure 13: Gene expression levels of BCAA catabolism-related genes in scWAT of RabGAP- deficient mice fed a HCLP or LCHP diet. qPCR analysis of the BCAA catabolism-related genes: branched-chain amino acid transaminase 1 (*Bcat1*) (A), branched-chain amino acid transaminase 2 (*Bcat2*) (B), branched-chain keto acid dehydrogenase E1 subunit beta (*Bckdhb*) (C), dihydrolipoamide branched-chain transacylase E2 *(Dbt)* (D), solute

carrier family 43 member 2 *(Slc43a2)* (E) and solute carrier family 7 member 5 *(Slc7a5)* (F) in WT, D1KO, D4KO and D1/D4KO mice fed a HCLP or LCHP diet. Expression levels were normalized to the housekeeping gene *18S rRNA*. Data are presented as mean ± SEM (n = 5-8) and were analyzed using two-way ANOVA with Bonferroni's multiple comparisons test. HCLP = high-carbohydrate low-protein diet, LCHP = low-carbohydrate high-protein diet.

3.2.6 Expression levels of pyruvate dehydrogenase complex in RabGAP-deficient mice after LCHP- or HCLP-feeding

The pyruvate dehydrogenase complex regulates glucose metabolism and is responsible for metabolic flexibility (Zhang et al., 2014), and BCAAs are inhibitors of this complex. Therefore, it was of interest to investigate the effect of HCLP and LCHP diets on the metabolic flexibility in RabGAP-deficient mice. For this purpose, qPCR analyses were conducted on scWAT from RabGAP-deficient mice fed HCLP or LCHP diets.

The analysis revealed that the HCLP diet resulted in higher gene expression levels of pyruvate dehydrogenase E1 subunit alpha 1 (*Pdha1*) compared to the LCHP diet (Figure 14 A). When comparing the *Pdha1* gene expression levels of the different genotypes on the HCLP diet, it was observed that D4KO mice showed lower gene expression levels compared to WT, D1KO, and D1/D4KO mice. However, this difference was not statistically significant (Figure 14 A). Pyruvate dehydrogenase E1 subunit beta (*Pdhb*) gene expression levels in WT (LP: 2.803 ± 1.227 vs. HP: 0.743 ± 0.216 p-value = 0.06), D1KO (LP: 1.473 ± 0.624 vs. HP: 0.621 ± 0.293), and D1/D4KO mice (LP: 1.211 ± 0.596 vs. HP: 0.650 ± 0.219) were lower on the LCHP diet compared to the HCLP diet (Figure 14 B). However, there was no significant increase in the gene expression levels of *Pdhb* in D4KO mice on the LCHP diet compared to the HCLP diet (LP: 0.301 ± 0.099 vs. HP: 0.920 ± 0.405) (Figure 14 B). The HCLP diet resulted in lower *Pdhb* gene expression levels in D4KO mice compared to WT, D1KO, and D1/D4KO mice, especially significantly lower levels compared to WT mice (Figure 14 B). The gene expression levels of pyruvate dehydrogenase complex component X (*Pdhx*) were increased overall on the HCLP diet in comparison to the LCHP diet (Figure 14 C). Furthermore, WT mice on the HCLP diet exhibited higher *Pdhx* gene expression levels compared to RabGAP-deficient mice (Figure 14 C).

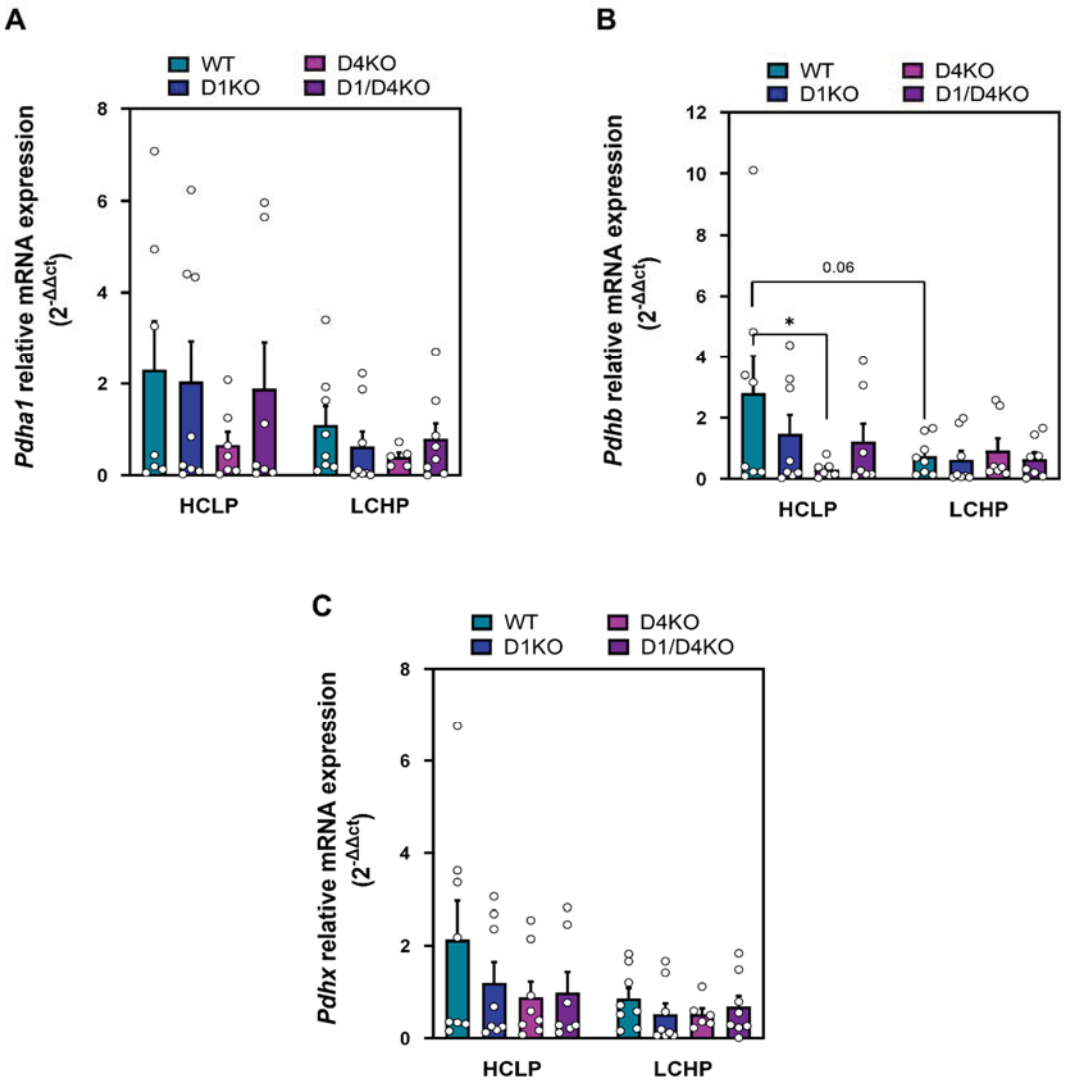

Figure 14: Gene expression levels of subunits of the pyruvate dehydrogenase complex in scWAT of RabGAP-deficient mice fed a HCLP or LCHP diet. Gene expression levels of subunits of the pyruvate dehydrogenase complex in scWAT of RabGAP-deficient mice. qPCR analysis of pyruvate dehydrogenase E1 subunit alpha 1 (*Pdha1*) (A), pyruvate dehydrogenase E1 subunit beta (*Pdhb*) (B) and pyruvate dehydrogenase complex component X (*Pdhx*) (C) in WT, D1KO, D4KO and D1/D4KO mice fed either a HCLP or a LCHP diet. Expression levels were normalized to the housekeeping gene *18S rRNA*. Data are presented as mean ± SEM (n = 5-8) and were analyzed using two-way ANOVA with Bonferroni's multiple comparisons test. *, $p < 0.05$ between indicated groups. HCLP = high-carbohydrate low-protein diet, LCHP = low-carbohydrate high-protein diet.

4 Discussion

Mutations in the RabGTPase-activating proteins (RabGAPs) TBC1D1 and TBC1D4, which play an important role in controlling energy substrate metabolism in skeletal muscle and adipose tissues, have been associated with the development of severe metabolic diseases in humans (Mafakheri et al., 2018, Espelage et al., 2020). A coding variant in *TBC1D1*, R125W, has been linked to severe familial obesity (Stone et al., 2006, Meyre et al., 2008), while a premature stop mutation, R363X, in *TBC1D4* leads to extreme postprandial hyperinsulinemia (Dash et al., 2009). Studies on RabGAP-deficient mice have shown impaired insulin-stimulated glucose uptake and enhanced fatty acid utilization, indicating a shift from glucose to lipids as the primary fuel source (Benninghoff et al., 2020, Chadt et al., 2015). Therefore, TBC1D1 and TBC1D4 are crucial for regulating glucose transport and promoting metabolic flexibility, which allows adaptation and switching of fuel oxidation based on fuel availability (Espelage et al., 2020). More recently, a loss-of-function mutation in the *TBC1D4* gene has been identified in several Arctic populations, which is associated with postprandial hyperglycemia and an increased risk of type 2 diabetes (T2DM) (Moltke et al., 2014). The traditional diet of indigenous Inuit populations is characterized by a low proportion of carbohydrates and a high protein and fat content. Lifestyle changes, in particular a reduction in physical activity and a westernized diet with high contents of carbohydrates and saturated fat, have dramatically increased the incidence of T2DM and cardiovascular disease (CVD) in these populations over the last decades (Moltke et al., 2014, Møller et al., 2021). Therefore, it was of interest to investigate the impact of a high diet with either protein or carbohydrate restriction on the expression profile and energy substrate metabolism in diabetes-relevant organs of RabGAP-deficient mice. Furthermore, we aimed to investigate the effects of nutrition on subcutaneous white adipose tissue (scWAT) browning since previous work of our research group has shown that regular exercise training, cold exposure, and stimulation of the β3-adrenergic receptor increase the expression levels of browning-related genes in D4KO mice (unpublished data). Therefore, this study used scWAT and liver samples of *Tbc1d1*-knockout (D1KO), *Tbc1d4*-knockout (D4KO), D1/D4KO, and wildtype (WT) mice that were previously fed high-fat diets with either a high amount of carbohydrate and a low amount of protein (referred to as the high-carb low-protein diet or HCLP), representing the Western diet, or *vice versa* (referred to as the low-carbohydrate high-protein diet or LCHP), representing the Arctic diet.

To investigate the impact of the respective diets on insulin-related glucose metabolism in the liver, Western blot analyses were performed. Additionally, the impact of the mentioned diets on the expression profile of different browning markers and branched-chain amino acid (BCAA) metabolism in adipose tissue was examined using quantitative PCR.

4.1 Impact of diets with different carbohydrate and protein contents on the glucose metabolism in the liver of RabGAP-deficient mice

4.1.1 Dietary carbohydrate restriction leading to increased gluconeogenesis in RabGAP-deficient mice

As demonstrated in Figure 6, the protein abundance of the cytosolic Phosphoenolpyruvate carboxykinase 1 (PEPCK1) isoform was significantly increased in WT, D1KO, and D1/4KO mice on the LCHP diet compared to the HCLP diet. However, the mitochondrial PEPCK2 protein abundance was not affected by either diet or genotype.

The results suggest increased gluconeogenesis in both WT mice and RabGAP-deficient mice on a LCHP diet compared to a HCLP diet, as PEPCK1, a key enzyme of gluconeogenesis, showed increased protein abundance(Yu et al., 2021b, Hatting et al., 2018). This indicates that dietary carbohydrate restriction affects the PEPCK1 protein abundance more than PEPCK2 in both WT mice and RabGAP-deficient mice. Therefore, restricting dietary carbohydrates may lead to increased gluconeogenesis in both WT mice and RabGAP-deficient mice, potentially indicating higher insulin resistance in these animals. Previous studies have shown that on a standard diet, the expression of both PEPCK1 and PEPCK2 increased in the liver of D1KO, D4KO, and D1/4KO mice compared to WT mice (Chadt et al., 2015).

In line with the results of our study, mice and rats fed a high-protein diet showed increased PEPCK1 protein levels and increased gluconeogenesis compared to those fed a low-protein diet (Azzout-Marniche et al., 2007, Garcia-Caraballo et al., 2013). Wang et al. (2013) similarly observed that in the liver, a D4KO leads to insulin resistance and higher PEPCK expression, resulting in increased gluconeogenesis. Interestingly, it is shown in Figure 6 A that D4KO mice on a HCLP diet demonstrate higher PEPCK1 protein abundance and therefore increased gluconeogenesis compared to the other genotypes. This suggests that a Western diet, which is high in carbohydrates and low in protein, may have a higher and more negative impact on the insulin resistance of individuals with *Tbc1d4*-deficiency compared to the other genotypes.

4.1.2 Increased glycogen synthesis by dietary carbohydrate restriction in WT and D4KO mice

The results show that in WT mice, glycogen synthase (GS) protein abundance was significantly lower on a LCHP diet compared to a HCLP diet. However, in RabGAP-deficient mice, GS protein abundance was unaltered. D4KO mice on the HCLP diet showed a higher GS protein abundance than D1KO and D1/4KO mice. Furthermore, this study found higher phosphorylation (Ser^{641}) of GS in WT and D4KO mice on the LCHP diet. Glycogen synthase kinase-3 α (GSK3α) was also found to be more phosphorylated (Ser^{21}) in WT mice and RabGAP-deficient mice on the LCHP diet.

Since GS is a key enzyme of glycogen synthesis and is activated in its phosphorylated state, and GSK3α, which inhibits activated GS, is inactivated when phosphorylated (Sharabi et al., 2015, Roach et al., 2012), these findings suggest increased glycogen synthesis, particularly in WT and D4KO mice on a LCHP diet compared to a HCLP diet.

Previous studies have demonstrated that D1KO, D4KO, and D1/4KO mice on a standard diet had lower hepatic glycogen concentrations than WT mice and no significant differences in GS (Ser^{641}) and GSK3α (Ser^{21}) protein abundance and phosphorylation (Chadt et al., 2015).

Stepien et al. (2011) showed that a high-protein, low-carbohydrate diet increases the expression levels of GS in rats, which may help maintain the relative stability of hepatic glycogen and suggest a progressive stimulation of glycogen synthesis. These findings are consistent with the results of this study, which suggest that carbohydrate restriction leads to higher glycogen synthesis in both WT mice and D4KO mice.

Another interesting observation is that D4KO mice on a HCLP diet show a lower phosphorylated GS ratio compared to the other genotypes, indicating reduced glycogen synthesis. This suggests that D4KO mice are more susceptible to the negative effects of a Western diet and that the combination of a *Tbc1d4*-deficiency and a Western diet may have more adverse effects, possibly because *Tbc1d4*-deficiency leads to impaired glucose uptake and disposal (Hargett et al., 2016), and the addition of excessive carbohydrates from a Western diet further disrupts glucose homeostasis.

4.2 Impact of diets with different carbohydrate and protein contents on the gene expression profile and energy substrate metabolism in scWAT of RabGAP-deficient mice

4.2.1 Dietary composition affects gene expression of specific browning markers

The gene expression levels of the browning markers *Ucp1*, *Cidea*, *Cox8b*, and *P2rx5* were significantly higher in WT mice fed a HCLP diet compared to a LCHP diet. This analysis revealed that the gene expression levels of specific browning markers may be affected by dietary composition, and a HCLP diet could increase the browning process in WT mice.

These results are consistent with previous studies that have also found that dietary protein restriction leads to increased *Fgf21* gene expression levels in the liver and elevated FGF21 circulation, which in turn stimulates the browning of WAT by increasing UCP1 expression levels (Pérez-Martí et al., 2017, Laeger et al., 2014, Aleman et al., 2019). The higher hepatic expression levels of FGF21 after a protein intake restriction were observed in both mice and rats (Laeger et al., 2014).

FGF21 is expressed in multiple tissues, however, increased hepatic synthesis and secretion of FGF21 has been shown to affect the brain, liver, and adipose tissue (Laeger et al., 2014). Therefore, higher *Fgf21* gene expression levels in the liver could affect adipose tissue without necessarily showing higher

Fgf21 gene expression levels in that tissue. This might also explain why, in this study, there were no increased expression levels of *Fgf21* in the adipose tissue of WT mice on the HCLP diet observable (Figure 9 B).

Yu et al. (2021a) also found that low-protein diets have beneficial effects on metabolic health in rodents and humans, specifically by reducing dietary intake of the BCAAs isoleucine and valine. The benefits of a low isoleucine diet include increased hepatic insulin sensitivity and ketogenesis, increased energy expenditure, activation of the FGF21-UCP1 axis, and reprogramming of liver and adipose metabolism. Similarly, a low valine intake induces metabolic effects similar to those stated above, but to a lesser extent than isoleucine. Interestingly, these effects are not observed with a low leucine diet. Reducing isoleucine and valine has been shown to rapidly restore metabolic health in diet-induced obese mice. Therefore, Yu et al. (2021a) consider isoleucine a key regulator of metabolic health and suggest reducing dietary isoleucine intake as a possible solution to treat and prevent obesity and diabetes.

In contrast to previous studies, Ma et al. (2020) stated that the dietary intake of the BCAAs leucine and isoleucine stimulates WAT browning in mice and could be helpful for the treatment of obesity.

4.2.2 *Tbc1d1* and *Tbc1d4* acting as possible diet-dependent regulators of browning

The results show that the gene expression levels of the browning markers *Pargc1a*, *Fgf21*, *Prdm16*, and *Pdgfra* (Figure 10 A, B, C, D) were lower in D1KO mice on the LCHP diet than on the HCLP diet. Conversely, the gene expression levels of *Cd137 and Bmp7* (Figure 10 E, F) were higher in D1KO mice on the LCHP diet than on the HCLP diet.

The results suggest a potential relevance of *Tbc1d1* in regulating the expression of specific browning markers under a LCHP diet compared to a HCLP diet. *Tbc1d1*-deficiency appears to lead to slightly reduced expression levels of *Ppargc1α, Fgf21*, and *Prdm16*, and slightly increased expression levels of *Cd137* and *Bmp7* on a LCHP diet compared to a HCLP diet.

Furthermore, the results demonstrated in Figure 10 indicate that gene expression levels of *P2rx5, Cidea*, *Cox8b,* and *Ucp1* were lower in D4KO mice on the HCLP diet compared to WT, D1KO, and D1/4KO mice. Additionally, it was seen that the gene expression levels of these browning markers were slightly higher on the HCLP diet compared to the LCHP diet in D4KO mice.

Tbc1d4-deficiency leads to decreased expression levels of *Cidea*, *P2rx5*, *Cox8b*, and *Ucp1* on a HCLP diet. The findings suggest that *Tbc1d4* is more relevant in regulating the expression of specific browning markers under HCLP diet feeding compared to a LCHP diet.

The study results show that the gene expression levels of the WAT marker *Wdnm1-like* were significantly higher in WT and D4KO mice on the LCHP diet compared to D1KO and D1/4KO mice. This suggests a reduction in whitening and an increase in browning in D1KO and D1/4KO mice under a LCHP diet, which is also evident in the gene expression levels of *Cd137*.

The precise mechanisms by which RabGAPs influence browning remain incompletely understood. Browning of WAT involves the upregulation of thermogenic genes, including *UCP1*, *PPARγ*, and *PRDM16* (Machado et al., 2022). RabGAPs participate in various cellular processes, such as vesicle trafficking and metabolic signaling (Stenmark, 2009). Consequently, RabGAPs may modulate signaling pathways that activate thermogenic genes by affecting vesicle trafficking and the membrane localization of receptors or transcription factors involved in browning.

Some Rab proteins, including Rab8a, Rab3d, and Rab35, contribute to the regulation of lipid storage and adipocyte function (Wang et al., 2022, Wu et al., 2014, López-Alcalá et al., 2024). These proteins could impact browning by influencing lipid dynamics within adipocytes. Notably, TBC1D4, a GTPase of Rab8a, plays a positive role in lipid droplet fusion and growth (Wu et al., 2014). The size of lipid droplets has been associated with obesity and hepatic steatosis, characterized by excessive fat accumulation in adipose tissues and the liver.

Despite the low expression levels of TBC1D1 in adipose tissue, its effects on glucose and lipid metabolism in skeletal muscle may indirectly influence adipocyte metabolism. By modulating Rab GTPase signaling pathways involved in adipocyte function, TBC1D1 could impact energy homeostasis and substrate utilization in adipose tissue (Chadt et al., 2008, Dokas et al., 2013, Stöckli et al., 2015). The deletion of RabGAPs *Tbc1d1* and *Tbc1d4* in mice has been shown to result in increased uptake and oxidation of long-chain fatty acids in skeletal muscle (Chadt et al., 2008, Chadt et al., 2015, Benninghoff et al., 2020). These metabolic changes may contribute to browning by increasing energy expenditure and promoting thermogenesis (Calderon-Dominguez et al., 2016, Gonzalez-Hurtado et al., 2018)

4.2.3 Carbohydrate-restrictive diet leading to lower *Slc2a4* gene expression levels in adipose tissue

The results of this study indicate that the gene expression levels of the gene of GLUT4, *Slc2a4,* in WT, D1KO, and D1/4KO mice were higher on a HCLP diet compared to a LCHP diet. Furthermore, WT mice on the HCLP diet exhibited significantly higher gene expression levels than D1KO and D4KO mice.

Considering the crucial role of TBC1D1 and TBC1D4 in insulin-stimulated glucose uptake and GLUT4 translocation, and the fact that RabGAP-deficiency leads to impaired glucose uptake (Lansey et al., 2012, Dokas et al., 2013), lower gene expression levels of the *Slc2a4* gene on both HCLP and LCHP diets could indicate a reduction in glucose uptake in adipose tissue. A prior study observed a significantly higher GLUT4 protein abundance in the tibialis anterior muscle of D4KO mice fed a LCHP diet compared to a HCLP diet (Master thesis Svenja Saurbier, 2021). This demonstrates tissue-dependent differences that could be due to the varying expression pattern of TBC1D1 in different tissues, as TBC1D1 is highly expressed in the tibialis anterior muscle but nearly absent in adipose tissue (Chadt et al., 2008). Additionally, it is suggested that increased dietary protein intake may specifically

affect, TBC1D1, leading to the promotion of processes that increase the abundance of GLUT4 protein. High-protein diets have also previously been associated with improved insulin sensitivity (Zhang et al., 2007).

Furthermore, the results suggest that RabGAP-deficient mice, particularly D4KO mice, are more negatively impacted by a HCLP diet than WT mice. This may be due to the inability to effectively utilize and dispose of the increased glucose intake from a HCLP diet in the presence of impaired insulin-stimulated Glut4 translocation and disrupted glucose disposal caused by the RabGAP-deficiency. (Chadt et al., 2015, Hargett et al., 2016, Stöckli et al., 2015). This may also explain the changes in the *TBC1D4*-deficient Inuit population, in which the higher prevalence of diabetes has become more apparent in the last decades, along with more westernized lifestyle changes such as consuming a HCLP diet (Moltke et al., 2014, Møller et al., 2021).

Interestingly, on a HCLP diet, mice with combined inactivation of *Tbc1d1* and *Tbc1d4* were observed to have higher *Slc2a4* gene expression levels than mice lacking either *Tbc1d1* or *Tbc1d4,* which may indicate a beneficial connection of a HCLP diet for D1/4KO mice compared to the effect of this diet on D1KO and D4KO mice. This observation may be attributed to the increased metabolic flexibility of the D1/4KO mice resulting from the combined inactivation of *Tbc1d1* and *Tbc1d4*, which may have triggered a metabolic shift toward increased lipid utilization, similar to what was observed in an adipose- and muscle-specific GLUT4-double KO (AMG4KO) mouse model. Metabolic adaptation, mediated by the upregulation of several enzymes, allowed the AMG4KO mice to maintain glucose homeostasis to a similar extent as the single GLUT4 knockout mice (Bickel, 2004). The D1/4KO mice may have undergone a comparable metabolic shift, explaining the observed higher *Slc2a4* gene expression levels compared to D1KO or D4KO mice. The HCLP diet may have further enhanced this adaptive response in D1/4KO mice.

4.2.4 Protein source and BCAA amount might play a relevant role in the metabolic effects of a high-protein diet

The study found that *Bcat2* gene expression levels were lower in RabGAP-deficient mice on a LCHP diet compared to WT mice. Additionally, both WT and RabGAP-deficient mice showed lower *Bckdhb* gene expression levels on a LCHP diet. These results contradict the expectation that a high-protein diet would increase *Bckdhb* gene expression levels, as BCKDHB is an important enzyme in BCAA catabolism.

The BCAA intake on the LCHP diet is higher than on the HCLP diet, however, gene expression levels of BCAA catabolism do not differ between the two diets. Therefore, it can be assumed that there are increased levels of unmetabolized BCAAs in cells and circulating in the blood. Previous studies have linked increased BCAA levels to obesity and certain metabolic disorders, such as impaired insulin

sensitivity (Kitada et al., 2019). Observational studies have associated better health and reduced mortality with low protein intake in humans (Levine et al., 2014).

Solon-Biet et al. (2015) found that *ad libitum*-fed HCLP diets improved lifespan and metabolic parameters such as insulin, glucose, and blood lipids in mice. Conversely, a LCHP diet was associated with higher mortality, cardiovascular disease, and diabetes mellitus (Lagiou et al., 2012, Fontana and Partridge, 2015). Interestingly, Solon-Biet et al. (2015) found that caloric restriction mice could prevent the negative metabolic consequences of a LCHP diet in *ad libitum*-fed mice. Fontana et al. (2016) suggest that a diet high in proteins containing a low amount of BCAAs would demonstrate the metabolic benefits of a protein-restricted diet.

In contrast, Wojcik et al. (2016) found that a high-protein diet with a mixed source from animals and plants had beneficial effects on insulin resistance and hepatic steatosis, independent of caloric intake, indicating the importance of the protein source. Stentz et al. (2016) reported a 100% remission of pre-diabetes to normal glucose tolerance by consuming a high-protein diet. In contrast, consuming a high-carbohydrate diet allowed only 33% remission. The protein source of the LCHP diet used in this study is mainly from casein, which is animal-based and high in BCAAs. Previous findings suggest the protein source and amount of BCAAs play a relevant role in the metabolic effects of a high-protein diet. This link may extend to RabGAP-deficient mice and could influence the metabolic adaptations that occur in response to RabGAP-deficiency. There is also growing evidence that TBC1D1 plays a crucial role in skeletal muscle development and is associated with meat production traits in various livestock species, indicating its important role in muscle biology (Espelage et al., 2020). It is possible that the source of protein and the amount of BCAAs may influence muscle cell development and differentiation, possibly by modifying signaling pathways that regulate TBC1D1 expression and function.

4.3 Conclusion and outlook

This research aimed to analyze the impact of two high-fat diets, with different carbohydrate and protein contents, representing the Western and Arctic diets, on the expression profile and energy substrate metabolism in diabetes-relevant organs in RabGAP-deficient mice. The study results suggest that *Tbc1d1* and *Tbc1d4* may act as diet-dependent regulators of browning. *Tbc1d4* may be more relevant in regulating the expression of browning markers under the HCLP diet, while *Tbc1d1* may be more relevant under the LCHP diet feeding. Additionally, the findings suggest that glucose homeostasis appears to be more affected by dietary carbohydrate restriction, leading to increased gluconeogenesis in RabGAP-deficient mice and increased glycogen synthesis in WT and D4KO mice.

Notably, the *Tbc1d4*-deficient mice are more negatively affected by a HCLP or Western diet compared to the other genotypes. This suggests that *Tbc1d4*-deficiency has a higher and more negative impact on insulin resistance. The higher prevalence of diabetes in the *TBC1D4*-deficient Inuit population in the last decades may be explained by the more westernized lifestyle changes, such as consuming a HCLP diet.

However, it should be noted the present study has several limitations. Caution must be applied due to the limited sample size, as the findings may not show a clear trend because of the interindividual biological differences of the mice. Therefore, a larger sample size, such as n=12, might help to confirm trends more clearly.

Additionally, since each animal is unique and the amount and structure of adipose tissue varies individually, we cannot be certain that the exact same amount of fat cells were used in each experiment, despite the use of the same mass.

For future research, conducting a citrate synthase assay could provide valuable insight. This analysis would allow for the assessment of mitochondrial content in the samples. This information could be used to determine whether the observed increased browning is attributable to an elevated mitochondrial content.

FGF21 is an important metabolic regulator in different pathways, and previous studies have shown increased FGF21 levels after consuming a low-protein diet. Therefore, it would be interesting to further investigate the role of FGF21 in RabGAP-deficient mice. To this end, Western blot analyses could be conducted to investigate the protein abundance of FGF21 and qPCR analyses to determine *Fgf21* gene expression in the liver.

Previous studies have shown that the protein source and amount of BCAAs may play a relevant role in the metabolic effects of a high-protein diet and insulin resistance. Therefore, it would be interesting to investigate the impact of high-protein diets with different amino acid components and from different sources on metabolic health in connection with RabGAP-deficiency.

Furthermore, as some studies suggest sex-specific benefits of reduced dietary BCAA intake in mice, it may also be beneficial to investigate the impact of different dietary carbohydrate and protein contents on female mice to be able to rule out sex-specific effects, since the mice used in this current study were all male. Additionally, further research is necessary to gain a complete understanding of how the protein source and amount of BCAAs affect the function and expression of RabGAPs.

5 Literature

ADEVA-ANDANY, M. M., GONZALEZ-LUCAN, M., FERNANDEZ-FERNANDEZ, C., CARNEIRO-FREIRE, N., SECO-FILGUEIRA, M. & PEDRE-PINEIRO, A. M. 2019. Effect of diet composition on insulin sensitivity in humans. *Clin Nutr ESPEN,* 33**,** 29-38.

ADEVA-ANDANY, M. M., PÉREZ-FELPETE, N., FERNÁNDEZ-FERNÁNDEZ, C., DONAPETRY-GARCÍA, C. & PAZOS-GARCÍA, C. 2016. Liver glucose metabolism in humans. *Biosci Rep,* 36.

ALEMAN, G., CASTRO, A. L., VIGIL-MARTINEZ, A., TORRE-VILLALVAZO, I., DIAZ-VILLASENOR, A., NORIEGA, L. G., MEDINA-VERA, I., ORDAZ, G., TORRES, N. & TOVAR, A. R. 2019. Interaction between the amount of dietary protein and the environmental temperature on the expression of browning markers in adipose tissue of rats. *Genes Nutr,* 14**,** 19.

AZZOUT-MARNICHE, D., GAUDICHON, C., BLOUET, C., BOS, C., MATHÉ, V., HUNEAU, J. F. & TOMÉ, D. 2007. Liver glyconeogenesis: a pathway to cope with postprandial amino acid excess in high-protein fed rats? *Am J Physiol Regul Integr Comp Physiol,* 292**,** R1400-7.

BARGUT, T. C., AGUILA, M. B. & MANDARIM-DE-LACERDA, C. A. 2016. Brown adipose tissue: Updates in cellular and molecular biology. *Tissue Cell,* 48**,** 452-60.

BARGUT, T. C. L., SOUZA-MELLO, V., AGUILA, M. B. & MANDARIM-DE-LACERDA, C. A. 2017. Browning of white adipose tissue: lessons from experimental models. *Hormone Molecular Biology and Clinical Investigation,* 31.

BAYS, H. E., GONZÁLEZ-CAMPOY, J. M., BRAY, G. A., KITABCHI, A. E., BERGMAN, D. A., SCHORR, A. B., RODBARD, H. W. & HENRY, R. R. 2008. Pathogenic potential of adipose tissue and metabolic consequences of adipocyte hypertrophy and increased visceral adiposity. *Expert Rev Cardiovasc Ther,* 6**,** 343-68.

BENNINGHOFF, T., ESPELAGE, L., EICKELSCHULTE, S., ZEINERT, I., SINOWENKA, I., MÜLLER, F., SCHÖNDELING, C., BATCHELOR, H., CAMES, S., ZHOU, Z., KOTZKA, J., CHADT, A. & AL-HASANI, H. 2020. The RabGAPs TBC1D1 and TBC1D4 Control Uptake of Long-Chain Fatty Acids Into Skeletal Muscle via Fatty Acid Transporter SLC27A4/FATP4. *Diabetes,* 69**,** 2281-2293.

BICKEL, P. E. 2004. Metabolic fuel selection: the importance of being flexible. *J Clin Invest,* 114**,** 1547-9.

BOUTARI, C. & MANTZOROS, C. S. 2022. A 2022 update on the epidemiology of obesity and a call to action: as its twin COVID-19 pandemic appears to be receding, the obesity and dysmetabolism pandemic continues to rage on. *Metabolism,* 133**,** 155217.

CALDERON-DOMINGUEZ, M., MIR, J. F., FUCHO, R., WEBER, M., SERRA, D. & HERRERO, L. 2016. Fatty acid metabolism and the basis of brown adipose tissue function. *Adipocyte,* 5**,** 98-118.

CHADT, A., IMMISCH, A., DE WENDT, C., SPRINGER, C., ZHOU, Z., STERMANN, T., HOLMAN, G. D., LOFFING-CUENI, D., LOFFING, J., JOOST, H. G. & AL-HASANI, H. 2015. "Deletion of both Rab-GTPase-activating proteins TBC1D1 and TBC1D4 in mice eliminates insulin- and AICAR-stimulated glucose transport [corrected]. *Diabetes,* 64**,** 746-59.

CHADT, A., LEICHT, K., DESHMUKH, A., JIANG, L. Q., SCHERNECK, S., BERNHARDT, U., DREJA, T., VOGEL, H., SCHMOLZ, K., KLUGE, R., ZIERATH, J. R., HULTSCHIG, C., HOEBEN, R. C., SCHÜRMANN, A., JOOST, H. G. & AL-HASANI, H. 2008. Tbc1d1 mutation in lean mouse strain confers leanness and protects from diet-induced obesity. *Nat Genet,* 40**,** 1354-9.

CHADT, A., SCHERNECK, S., JOOST, H. G. & AL-HASANI, H. 2018. Molecular links between Obesity and Diabetes: “Diabesity”. *In:* FEINGOLD, K. R., ANAWALT, B., BOYCE, A., CHROUSOS, G., DE HERDER, W. W., DHATARIYA, K., DUNGAN, K., HERSHMAN, J. M., HOFLAND, J., KALRA, S., KALTSAS, G., KOCH, C., KOPP, P., KORBONITS, M., KOVACS, C. S., KUOHUNG, W., LAFERRÈRE, B., LEVY, M., MCGEE, E. A., MCLACHLAN, R., MORLEY, J. E., NEW, M., PURNELL, J., SAHAY, R., SINGER, F.,

SPERLING, M. A., STRATAKIS, C. A., TRENCE, D. L. & WILSON, D. P. (eds.) *Endotext.* South Dartmouth (MA): MDText.com, Inc.

Copyright © 2000-2022, MDText.com, Inc.

CHATTERJEE, S., KHUNTI, K. & DAVIES, M. J. 2017. Type 2 diabetes. *Lancet,* 389**,** 2239-2251.

CHOUCHANI, E. T., KAZAK, L. & SPIEGELMAN, B. M. 2019. New Advances in Adaptive Thermogenesis: UCP1 and Beyond. *Cell Metab,* 29**,** 27-37.

CHUSYD, D. E., WANG, D., HUFFMAN, D. M. & NAGY, T. R. 2016. Relationships between Rodent White Adipose Fat Pads and Human White Adipose Fat Depots. *Front Nutr,* 3**,** 10.

DASH, S., SANO, H., ROCHFORD, J. J., SEMPLE, R. K., YEO, G., HYDEN, C. S., SOOS, M. A., CLARK, J., RODIN, A., LANGENBERG, C., DRUET, C., FAWCETT, K. A., TUNG, Y. C., WAREHAM, N. J., BARROSO, I., LIENHARD, G. E., O'RAHILLY, S. & SAVAGE, D. B. 2009. A truncation mutation in TBC1D4 in a family with acanthosis nigricans and postprandial hyperinsulinemia. *Proc Natl Acad Sci U S A,* 106**,** 9350-5.

DE JONG, J. M., LARSSON, O., CANNON, B. & NEDERGAARD, J. 2015. A stringent validation of mouse adipose tissue identity markers. *Am J Physiol Endocrinol Metab,* 308**,** E1085-105.

DEFRONZO, R. A., FERRANNINI, E., GROOP, L., HENRY, R. R., HERMAN, W. H., HOLST, J. J., HU, F. B., KAHN, C. R., RAZ, I., SHULMAN, G. I., SIMONSON, D. C., TESTA, M. A. & WEISS, R. 2015. Type 2 diabetes mellitus. *Nat Rev Dis Primers,* 1**,** 15019.

DOKAS, J., CHADT, A., JOOST, H. G. & AL-HASANI, H. 2016. Tbc1d1 deletion suppresses obesity in leptin-deficient mice. *Int J Obes (Lond),* 40**,** 1242-9.

DOKAS, J., CHADT, A., NOLDEN, T., HIMMELBAUER, H., ZIERATH, J. R., JOOST, H. G. & AL-HASANI, H. 2013. Conventional knockout of Tbc1d1 in mice impairs insulin- and AICAR-stimulated glucose uptake in skeletal muscle. *Endocrinology,* 154**,** 3502-14.

EICKELSCHULTE, S., HARTWIG, S., LEISER, B., LEHR, S., JOSCHKO, V., CHOKKALINGAM, M., CHADT, A. & AL-HASANI, H. 2021. AKT/AMPK-mediated phosphorylation of TBC1D4 disrupts the interaction with insulin-regulated aminopeptidase. *J Biol Chem,* 296**,** 100637.

ESPELAGE, L., AL-HASANI, H. & CHADT, A. 2020. RabGAPs in skeletal muscle function and exercise. *J Mol Endocrinol,* 64**,** R1-R19.

FASELIS, C., KATSIMARDOU, A., IMPRIALOS, K., DELIGKARIS, P., KALLISTRATOS, M. & DIMITRIADIS, K. 2020. Microvascular Complications of Type 2 Diabetes Mellitus. *Curr Vasc Pharmacol,* 18**,** 117-124.

FONTANA, L., CUMMINGS, N. E., ARRIOLA APELO, S. I., NEUMAN, J. C., KASZA, I., SCHMIDT, B. A., CAVA, E., SPELTA, F., TOSTI, V., SYED, F. A., BAAR, E. L., VERONESE, N., COTTRELL, S. E., FENSKE, R. J., BERTOZZI, B., BRAR, H. K., PIETKA, T., BULLOCK, A. D., FIGENSHAU, R. S., ANDRIOLE, G. L., MERRINS, M. J., ALEXANDER, C. M., KIMPLE, M. E. & LAMMING, D. W. 2016. Decreased Consumption of Branched-Chain Amino Acids Improves Metabolic Health. *Cell Reports,* 16**,** 520-530.

FONTANA, L. & PARTRIDGE, L. 2015. Promoting health and longevity through diet: from model organisms to humans. *Cell,* 161**,** 106-118.

FRANK, A. P., DE SOUZA SANTOS, R., PALMER, B. F. & CLEGG, D. J. 2019. Determinants of body fat distribution in humans may provide insight about obesity-related health risks. *J Lipid Res,* 60**,** 1710-1719.

FRIGOLET, M. E. & GUTIÉRREZ-AGUILAR, R. 2020. The colors of adipose tissue. *Gac Med Mex,* 156**,** 142-149.

GALICIA-GARCIA, U., BENITO-VICENTE, A., JEBARI, S., LARREA-SEBAL, A., SIDDIQI, H., URIBE, K. B., OSTOLAZA, H. & MARTÍN, C. 2020. Pathophysiology of Type 2 Diabetes Mellitus. *Int J Mol Sci,* 21.

GARCIA-CARABALLO, S. C., COMHAIR, T. M., VERHEYEN, F., GAEMERS, I., SCHAAP, F. G., HOUTEN, S. M., HAKVOORT, T. B., DEJONG, C. H., LAMERS, W. H. &

KOEHLER, S. E. 2013. Prevention and reversal of hepatic steatosis with a high-protein diet in mice. *Biochim Biophys Acta,* 1832**,** 685-95.
GARCIA, R. A., ROEMMICH, J. N. & CLAYCOMBE, K. J. 2016. Evaluation of markers of beige adipocytes in white adipose tissue of the mouse. *Nutr Metab (Lond),* 13**,** 24.
GONZALEZ-HURTADO, E., LEE, J., CHOI, J. & WOLFGANG, M. J. 2018. Fatty acid oxidation is required for active and quiescent brown adipose tissue maintenance and thermogenic programing. *Mol Metab,* 7**,** 45-56.
GREGG, E. W., SATTAR, N. & ALI, M. K. 2016. The changing face of diabetes complications. *Lancet Diabetes Endocrinol,* 4**,** 537-47.
GUO, P., LI, Y., ESLAMFAM, S., DING, W. & MA, X. 2017. Discovery of Novel Genes Mediating Glucose and Lipid Metabolisms. *Curr Protein Pept Sci,* 18**,** 609-618.
HARGETT, S. R., WALKER, N. N. & KELLER, S. R. 2016. Rab GAPs AS160 and Tbc1d1 play nonredundant roles in the regulation of glucose and energy homeostasis in mice. *Am J Physiol Endocrinol Metab,* 310**,** E276-88.
HARMS, M. J., ISHIBASHI, J., WANG, W., LIM, H. W., GOYAMA, S., SATO, T., KUROKAWA, M., WON, K. J. & SEALE, P. 2014. Prdm16 is required for the maintenance of brown adipocyte identity and function in adult mice. *Cell Metab,* 19**,** 593-604.
HATTING, M., TAVARES, C. D. J., SHARABI, K., RINES, A. K. & PUIGSERVER, P. 2018. Insulin regulation of gluconeogenesis. *Ann N Y Acad Sci,* 1411**,** 21-35.
HEALD, A. H., STEDMAN, M., DAVIES, M., LIVINGSTON, M., ALSHAMES, R., LUNT, M., RAYMAN, G. & GADSBY, R. 2020. Estimating life years lost to diabetes: outcomes from analysis of National Diabetes Audit and Office of National Statistics data. *Cardiovasc Endocrinol Metab,* 9**,** 183-185.
HEWTON, K. G., JOHAL, A. S. & PARKER, S. J. 2021. Transporters at the Interface between Cytosolic and Mitochondrial Amino Acid Metabolism. *Metabolites,* 11**,** 112.
IBRAHIM, M. M. 2010. Subcutaneous and visceral adipose tissue: structural and functional differences. *Obes Rev,* 11**,** 11-8.
JENSEN, M. V., JOSEPH, J. W., RONNEBAUM, S. M., BURGESS, S. C., SHERRY, A. D. & NEWGARD, C. B. 2008. Metabolic cycling in control of glucose-stimulated insulin secretion. *Am J Physiol Endocrinol Metab,* 295**,** E1287-97.
KAHN, S. E., HULL, R. L. & UTZSCHNEIDER, K. M. 2006. Mechanisms linking obesity to insulin resistance and type 2 diabetes. *Nature,* 444**,** 840-6.
KAISER, A. B., ZHANG, N. & DER PLUIJM, W. V. 2018. Global Prevalence of Type 2 Diabetes over the Next Ten Years (2018-2028). *Diabetes,* 67.
KERSHAW, E. E. & FLIER, J. S. 2004. Adipose tissue as an endocrine organ. *J Clin Endocrinol Metab,* 89**,** 2548-56.
KITADA, M., OGURA, Y., MONNO, I. & KOYA, D. 2019. The impact of dietary protein intake on longevity and metabolic health. *EBioMedicine,* 43**,** 632-640.
KURYŁOWICZ, A. & PUZIANOWSKA-KUŹNICKA, M. 2020. Induction of Adipose Tissue Browning as a Strategy to Combat Obesity. *Int J Mol Sci,* 21.
LAEGER, T., HENAGAN, T. M., ALBARADO, D. C., REDMAN, L. M., BRAY, G. A., NOLAND, R. C., MÜNZBERG, H., HUTSON, S. M., GETTYS, T. W., SCHWARTZ, M. W. & MORRISON, C. D. 2014. FGF21 is an endocrine signal of protein restriction. *J Clin Invest,* 124**,** 3913-22.
LAGIOU, P., SANDIN, S., LOF, M., TRICHOPOULOS, D., ADAMI, H. O. & WEIDERPASS, E. 2012. Low carbohydrate-high protein diet and incidence of cardiovascular diseases in Swedish women: prospective cohort study. *Bmj,* 344**,** e4026.
LANSEY, M. N., WALKER, N. N., HARGETT, S. R., STEVENS, J. R. & KELLER, S. R. 2012. Deletion of Rab GAP AS160 modifies glucose uptake and GLUT4 translocation in primary skeletal muscles and adipocytes and impairs glucose homeostasis. *Am J Physiol Endocrinol Metab,* 303**,** E1273-86.
LEE, I. K. 2014. The role of pyruvate dehydrogenase kinase in diabetes and obesity. *Diabetes Metab J,* 38**,** 181-6.
LENEY, S. E. & TAVARÉ, J. M. 2009. The molecular basis of insulin-stimulated glucose uptake: signalling, trafficking and potential drug targets. *J Endocrinol,* 203**,** 1-18.

LERIN, C., GOLDFINE, A. B., BOES, T., LIU, M., KASIF, S., DREYFUSS, J. M., DE SOUSA-COELHO, A. L., DAHER, G., MANOLI, I., SYSOL, J. R., ISGANAITIS, E., JESSEN, N., GOODYEAR, L. J., BEEBE, K., GALL, W., VENDITTI, C. P. & PATTI, M. E. 2016. Defects in muscle branched-chain amino acid oxidation contribute to impaired lipid metabolism. *Mol Metab,* 5**,** 926-936.

LETO, D. & SALTIEL, A. R. 2012. Regulation of glucose transport by insulin: traffic control of GLUT4. *Nat Rev Mol Cell Biol,* 13**,** 383-96.

LEVINE, M. E., SUAREZ, J. A., BRANDHORST, S., BALASUBRAMANIAN, P., CHENG, C. W., MADIA, F., FONTANA, L., MIRISOLA, M. G., GUEVARA-AGUIRRE, J., WAN, J., PASSARINO, G., KENNEDY, B. K., WEI, M., COHEN, P., CRIMMINS, E. M. & LONGO, V. D. 2014. Low protein intake is associated with a major reduction in IGF-1, cancer, and overall mortality in the 65 and younger but not older population. *Cell Metab,* 19**,** 407-17.

LEY, S. H., HAMDY, O., MOHAN, V. & HU, F. B. 2014. Prevention and management of type 2 diabetes: dietary components and nutritional strategies. *Lancet,* 383**,** 1999-2007.

LI, T., ZHANG, Z., KOLWICZ, S. C., JR., ABELL, L., ROE, N. D., KIM, M., ZHOU, B., CAO, Y., RITTERHOFF, J., GU, H., RAFTERY, D., SUN, H. & TIAN, R. 2017. Defective Branched-Chain Amino Acid Catabolism Disrupts Glucose Metabolism and Sensitizes the Heart to Ischemia-Reperfusion Injury. *Cell Metab,* 25**,** 374-385.

LIN, J. C., TARN, W. Y. & HSIEH, W. K. 2014. Emerging role for RNA binding motif protein 4 in the development of brown adipocytes. *Biochim Biophys Acta,* 1843**,** 769-79.

LÓPEZ-ALCALÁ, J., GORDON, A., TRÁVEZ, A., TERCERO-ALCÁZAR, C., CORREA-SÁEZ, A., GONZÁLEZ-RELLÁN, M. J., RANGEL-ZÚÑIGA, O. A., RODRÍGUEZ, A., MEMBRIVES, A., FRÜHBECK, G., NOGUEIRAS, R., CALZADO, M. A., GUZMÁN-RUIZ, R. & MALAGÓN, M. M. 2024. Localization, traffic and function of Rab34 in adipocyte lipid and endocrine functions. *Journal of Biomedical Science,* 31**,** 2.

LOTTA, L. A., SCOTT, R. A., SHARP, S. J., BURGESS, S., LUAN, J., TILLIN, T., SCHMIDT, A. F., IMAMURA, F., STEWART, I. D., PERRY, J. R., MARNEY, L., KOULMAN, A., KAROLY, E. D., FOROUHI, N. G., SJÖGREN, R. J., NÄSLUND, E., ZIERATH, J. R., KROOK, A., SAVAGE, D. B., GRIFFIN, J. L., CHATURVEDI, N., HINGORANI, A. D., KHAW, K. T., BARROSO, I., MCCARTHY, M. I., O'RAHILLY, S., WAREHAM, N. J. & LANGENBERG, C. 2016. Genetic Predisposition to an Impaired Metabolism of the Branched-Chain Amino Acids and Risk of Type 2 Diabetes: A Mendelian Randomisation Analysis. *PLoS Med,* 13**,** e1002179.

MA, Q., ZHOU, X., HU, L., CHEN, J., ZHU, J. & SHAN, A. 2020. Leucine and isoleucine have similar effects on reducing lipid accumulation, improving insulin sensitivity and increasing the browning of WAT in high-fat diet-induced obese mice. *Food Funct,* 11**,** 2279-2290.

MA, Q. X., ZHU, W. Y., LU, X. C., JIANG, D., XU, F., LI, J. T., ZHANG, L., WU, Y. L., CHEN, Z. J., YIN, M., HUANG, H. Y. & LEI, Q. Y. 2022. BCAA-BCKA axis regulates WAT browning through acetylation of PRDM16. *Nat Metab,* 4**,** 106-122.

MACHADO, S. A., PASQUARELLI-DO-NASCIMENTO, G., DA SILVA, DEBORA S., FARIAS, G. R., DE OLIVEIRA SANTOS, I., BAPTISTA, L. B. & MAGALHÃES, K. G. 2022. Browning of the white adipose tissue regulation: new insights into nutritional and metabolic relevance in health and diseases. *Nutrition & Metabolism,* 19**,** 61.

MAFAKHERI, S., CHADT, A. & AL-HASANI, H. 2018. Regulation of RabGAPs involved in insulin action. *Biochem Soc Trans,* 46**,** 683-690.

MAHENDRAN, Y., JONSSON, A., HAVE, C. T., ALLIN, K. H., WITTE, D. R., JØRGENSEN, M. E., GRARUP, N., PEDERSEN, O., KILPELÄINEN, T. O. & HANSEN, T. 2017. Genetic evidence of a causal effect of insulin resistance on branched-chain amino acid levels. *Diabetologia,* 60**,** 873-878.

MANNING, B. D. & TOKER, A. 2017. AKT/PKB Signaling: Navigating the Network. *Cell,* 169**,** 381-405.

MANOUSAKI, D., KENT, J. W., JR., HAACK, K., ZHOU, S., XIE, P., GREENWOOD, C. M., BRASSARD, P., NEWMAN, D. E., COLE, S., UMANS, J. G., ROULEAU, G., COMUZZIE, A. G. & RICHARDS, J. B. 2016. Toward Precision Medicine: TBC1D4

Disruption Is Common Among the Inuit and Leads to Underdiagnosis of Type 2 Diabetes. *Diabetes Care,* 39**,** 1889-1895.

MEYRE, D., FARGE, M., LECOEUR, C., PROENCA, C., DURAND, E., ALLEGAERT, F., TICHET, J., MARRE, M., BALKAU, B., WEILL, J., DELPLANQUE, J. & FROGUEL, P. 2008. R125W coding variant in TBC1D1 confers risk for familial obesity and contributes to linkage on chromosome 4p14 in the French population. *Hum Mol Genet,* 17**,** 1798-802.

MITTAL, B. 2019. Subcutaneous adipose tissue & visceral adipose tissue. *Indian J Med Res,* 149**,** 571-573.

MØLLER, G., LIND, M. V., HAUPTMANN, A. L., SENFTLEBER, N., HANSEN, C. B., HANSEN, T., JØRGENSEN, M. E. & LAURITZEN, L. 2021. The role of a traditional and western diet on glucose homeostasis in Greenlandic Inuit carriers and non-carriers of type 2 diabetes variant in the TBC1D4 gene: A protocol for a randomized clinical trial. *Contemp Clin Trials Commun,* 21**,** 100734.

MOLTKE, I., GRARUP, N., JORGENSEN, M. E., BJERREGAARD, P., TREEBAK, J. T., FUMAGALLI, M., KORNELIUSSEN, T. S., ANDERSEN, M. A., NIELSEN, T. S., KRARUP, N. T., GJESING, A. P., ZIERATH, J. R., LINNEBERG, A., WU, X., SUN, G., JIN, X., AL-AAMA, J., WANG, J., BORCH-JOHNSEN, K., PEDERSEN, O., NIELSEN, R., ALBRECHTSEN, A. & HANSEN, T. 2014. A common Greenlandic TBC1D4 variant confers muscle insulin resistance and type 2 diabetes. *Nature,* 512**,** 190-3.

MUNCH-ANDERSEN, T., OLSEN, D. B., SØNDERGAARD, H., DAUGAARD, J. R., BYSTED, A., CHRISTENSEN, D. L., SALTIN, B. & HELGE, J. W. 2012. Metabolic profile in two physically active Inuit groups consuming either a western or a traditional Inuit diet. *Int J Circumpolar Health,* 71**,** 17342.

MURAWSKA-CIAŁOWICZ, E. 2017. Adipose tissue - morphological and biochemical characteristic of different depots. *Postepy Hig Med Dosw (Online),* 71**,** 466-484.

NAGY, C. & EINWALLNER, E. 2018. Study of In Vivo Glucose Metabolism in High-fat Diet-fed Mice Using Oral Glucose Tolerance Test (OGTT) and Insulin Tolerance Test (ITT). *J Vis Exp*.

NEWGARD, C. B., AN, J., BAIN, J. R., MUEHLBAUER, M. J., STEVENS, R. D., LIEN, L. F., HAQQ, A. M., SHAH, S. H., ARLOTTO, M., SLENTZ, C. A., ROCHON, J., GALLUP, D., ILKAYEVA, O., WENNER, B. R., YANCY, W. S., JR., EISENSON, H., MUSANTE, G., SURWIT, R. S., MILLINGTON, D. S., BUTLER, M. D. & SVETKEY, L. P. 2009. A branched-chain amino acid-related metabolic signature that differentiates obese and lean humans and contributes to insulin resistance. *Cell Metab,* 9**,** 311-26.

PENG, H., WANG, Y. & LUO, W. 2020. Multifaceted role of branched-chain amino acid metabolism in cancer. *Oncogene,* 39**,** 6747-6756.

PÉREZ-MARTÍ, A., GARCIA-GUASCH, M., TRESSERRA-RIMBAU, A., CARRILHO-DO-ROSÁRIO, A., ESTRUCH, R., SALAS-SALVADÓ, J., MARTÍNEZ-GONZÁLEZ, M., LAMUELA-RAVENTÓS, R., MARRERO, P. F., HARO, D. & RELAT, J. 2017. A low-protein diet induces body weight loss and browning of subcutaneous white adipose tissue through enhanced expression of hepatic fibroblast growth factor 21 (FGF21). *Mol Nutr Food Res,* 61.

PICHE, M. E., TCHERNOF, A. & DESPRES, J. P. 2020. Obesity Phenotypes, Diabetes, and Cardiovascular Diseases. *Circ Res,* 126**,** 1477-1500.

ROACH, P. J., DEPAOLI-ROACH, A. A., HURLEY, T. D. & TAGLIABRACCI, V. S. 2012. Glycogen and its metabolism: some new developments and old themes. *Biochem J,* 441**,** 763-87.

ROMERO-GÓMEZ, M. 2022. Non-alcoholic steatohepatitis. *Med Clin (Barc)*.

SAITO, M., MATSUSHITA, M., YONESHIRO, T. & OKAMATSU-OGURA, Y. 2020. Brown Adipose Tissue, Diet-Induced Thermogenesis, and Thermogenic Food Ingredients: From Mice to Men. *Front Endocrinol (Lausanne),* 11**,** 222.

SAITO, M., OKAMATSU-OGURA, Y., MATSUSHITA, M., WATANABE, K., YONESHIRO, T., NIO-KOBAYASHI, J., IWANAGA, T., MIYAGAWA, M., KAMEYA, T., NAKADA, K., KAWAI, Y. & TSUJISAKI, M. 2009. High incidence of metabolically active brown

adipose tissue in healthy adult humans: effects of cold exposure and adiposity. *Diabetes,* 58**,** 1526-31.
SAKAMOTO, K. & HOLMAN, G. D. 2008. Emerging role for AS160/TBC1D4 and TBC1D1 in the regulation of GLUT4 traffic. *Am J Physiol Endocrinol Metab,* 295**,** E29-37.
SCHEEL, A. K., ESPELAGE, L. & CHADT, A. 2022. Many Ways to Rome: Exercise, Cold Exposure and Diet-Do They All Affect BAT Activation and WAT Browning in the Same Manner? *Int J Mol Sci,* 23.
SEALE, P., BJORK, B., YANG, W., KAJIMURA, S., CHIN, S., KUANG, S., SCIMÈ, A., DEVARAKONDA, S., CONROE, H. M., ERDJUMENT-BROMAGE, H., TEMPST, P., RUDNICKI, M. A., BEIER, D. R. & SPIEGELMAN, B. M. 2008. PRDM16 controls a brown fat/skeletal muscle switch. *Nature,* 454**,** 961-7.
SHARABI, K., TAVARES, C. D., RINES, A. K. & PUIGSERVER, P. 2015. Molecular pathophysiology of hepatic glucose production. *Mol Aspects Med,* 46**,** 21-33.
SHE, P., VAN HORN, C., REID, T., HUTSON, S. M., COONEY, R. N. & LYNCH, C. J. 2007. Obesity-related elevations in plasma leucine are associated with alterations in enzymes involved in branched-chain amino acid metabolism. *Am J Physiol Endocrinol Metab,* 293**,** E1552-63.
SOLON-BIET, S. M., MITCHELL, S. J., COOGAN, S. C., COGGER, V. C., GOKARN, R., MCMAHON, A. C., RAUBENHEIMER, D., DE CABO, R., SIMPSON, S. J. & LE COUTEUR, D. G. 2015. Dietary Protein to Carbohydrate Ratio and Caloric Restriction: Comparing Metabolic Outcomes in Mice. *Cell Rep,* 11**,** 1529-34.
STENMARK, H. 2009. Rab GTPases as coordinators of vesicle traffic. *Nature Reviews Molecular Cell Biology,* 10**,** 513-525.
STENTZ, F. B., BREWER, A., WAN, J., GARBER, C., DANIELS, B., SANDS, C. & KITABCHI, A. E. 2016. Remission of pre-diabetes to normal glucose tolerance in obese adults with high protein versus high carbohydrate diet: randomized control trial. *BMJ Open Diabetes Research & Care,* 4**,** e000258.
STEPIEN, M., GAUDICHON, C., FROMENTIN, G., EVEN, P., TOMÉ, D. & AZZOUT-MARNICHE, D. 2011. Increasing protein at the expense of carbohydrate in the diet down-regulates glucose utilization as glucose sparing effect in rats. *PLoS One,* 6**,** e14664.
STÖCKLI, J., MEOLI, C. C., HOFFMAN, N. J., FAZAKERLEY, D. J., PANT, H., CLEASBY, M. E., MA, X., KLEINERT, M., BRANDON, A. E., LOPEZ, J. A., COONEY, G. J. & JAMES, D. E. 2015. The RabGAP TBC1D1 Plays a Central Role in Exercise-Regulated Glucose Metabolism in Skeletal Muscle. *Diabetes,* 64**,** 1914-1922.
STONE, S., ABKEVICH, V., RUSSELL, D. L., RILEY, R., TIMMS, K., TRAN, T., TREM, D., FRANK, D., JAMMULAPATI, S., NEFF, C. D., ILIEV, D., GRESS, R., HE, G., FRECH, G. C., ADAMS, T. D., SKOLNICK, M. H., LANCHBURY, J. S., GUTIN, A., HUNT, S. C. & SHATTUCK, D. 2006. TBC1D1 is a candidate for a severe obesity gene and evidence for a gene/gene interaction in obesity predisposition. *Hum Mol Genet,* 15**,** 2709-20.
SZEKERES, F., CHADT, A., TOM, R. Z., DESHMUKH, A. S., CHIBALIN, A. V., BJÖRNHOLM, M., AL-HASANI, H. & ZIERATH, J. R. 2012. The Rab-GTPase-activating protein TBC1D1 regulates skeletal muscle glucose metabolism. *Am J Physiol Endocrinol Metab,* 303**,** E524-33.
TATSUKAWA, Y., MISUMI, M., KIM, Y. M., YAMADA, M., OHISHI, W., FUJIWARA, S., NAKANISHI, S. & YONEDA, M. 2018. Body composition and development of diabetes: a 15-year follow-up study in a Japanese population. *Eur J Clin Nutr,* 72**,** 374-380.
THIRONE, A. C., HUANG, C. & KLIP, A. 2006. Tissue-specific roles of IRS proteins in insulin signaling and glucose transport. *Trends Endocrinol Metab,* 17**,** 72-8.
TOZZI, M. & NOVAK, I. 2017. Purinergic Receptors in Adipose Tissue As Potential Targets in Metabolic Disorders. *Front Pharmacol,* 8**,** 878.
VANWEERT, F., DE LIGT, M., HOEKS, J., HESSELINK, M. K. C., SCHRAUWEN, P. & PHIELIX, E. 2021. Elevated Plasma Branched-Chain Amino Acid Levels Correlate With Type 2 Diabetes-Related Metabolic Disturbances. *J Clin Endocrinol Metab,* 106**,** e1827-e1836.

VANWEERT, F., SCHRAUWEN, P. & PHIELIX, E. 2022. Role of branched-chain amino acid metabolism in the pathogenesis of obesity and type 2 diabetes-related metabolic disturbances BCAA metabolism in type 2 diabetes. *Nutr Diabetes,* 12**,** 35.

VERNOCHET, C., MCDONALD, M. E. & FARMER, S. R. 2010. Brown adipose tissue: a promising target to combat obesity. *Drug News Perspect,* 23**,** 409-17.

VIIGIMAA, M., SACHINIDIS, A., TOUMPOURLEKA, M., KOUTSAMPASOPOULOS, K., ALLIKSOO, S. & TITMA, T. 2020. Macrovascular Complications of Type 2 Diabetes Mellitus. *Curr Vasc Pharmacol,* 18**,** 110-116.

WANG, H. Y., DUCOMMUN, S., QUAN, C., XIE, B., LI, M., WASSERMAN, D. H., SAKAMOTO, K., MACKINTOSH, C. & CHEN, S. 2013. AS160 deficiency causes whole-body insulin resistance via composite effects in multiple tissues. *Biochem J,* 449**,** 479-89.

WANG, Q., HOLMES, M. V., DAVEY SMITH, G. & ALA-KORPELA, M. 2017. Genetic Support for a Causal Role of Insulin Resistance on Circulating Branched-Chain Amino Acids and Inflammation. *Diabetes Care,* 40**,** 1779-1786.

WANG, T., JIN, M. J. & LI, L. K. 2022. [The GTP-Bound form of Rab3D Promotes Lipid Droplet Growth in Adipocyte]. *Mol Biol (Mosk),* 56**,** 564-573.

WANG, T. J., LARSON, M. G., VASAN, R. S., CHENG, S., RHEE, E. P., MCCABE, E., LEWIS, G. D., FOX, C. S., JACQUES, P. F., FERNANDEZ, C., O'DONNELL, C. J., CARR, S. A., MOOTHA, V. K., FLOREZ, J. C., SOUZA, A., MELANDER, O., CLISH, C. B. & GERSZTEN, R. E. 2011. Metabolite profiles and the risk of developing diabetes. *Nat Med,* 17**,** 448-53.

WHITE, P. J., LAPWORTH, A. L., AN, J., WANG, L., MCGARRAH, R. W., STEVENS, R. D., ILKAYEVA, O., GEORGE, T., MUEHLBAUER, M. J., BAIN, J. R., TRIMMER, J. K., BROSNAN, M. J., ROLPH, T. P. & NEWGARD, C. B. 2016. Branched-chain amino acid restriction in Zucker-fatty rats improves muscle insulin sensitivity by enhancing efficiency of fatty acid oxidation and acyl-glycine export. *Mol Metab,* 5**,** 538-551.

WOJCIK, J. L., DEVASSY, J. G., WU, Y., ZAHRADKA, P., TAYLOR, C. G. & AUKEMA, H. M. 2016. Protein source in a high-protein diet modulates reductions in insulin resistance and hepatic steatosis in fa/fa Zucker rats. *Obesity (Silver Spring),* 24**,** 123-31.

WU, J., BOSTRÖM, P., SPARKS, L. M., YE, L., CHOI, J. H., GIANG, A. H., KHANDEKAR, M., VIRTANEN, K. A., NUUTILA, P., SCHAART, G., HUANG, K., TU, H., VAN MARKEN LICHTENBELT, W. D., HOEKS, J., ENERBÄCK, S., SCHRAUWEN, P. & SPIEGELMAN, B. M. 2012. Beige adipocytes are a distinct type of thermogenic fat cell in mouse and human. *Cell,* 150**,** 366-76.

WU, L., XU, D., ZHOU, L., XIE, B., YU, L., YANG, H., HUANG, L., YE, J., DENG, H., YUAN, Y. A., CHEN, S. & LI, P. 2014. Rab8a-AS160-MSS4 regulatory circuit controls lipid droplet fusion and growth. *Dev Cell,* 30**,** 378-93.

YONESHIRO, T., WANG, Q., TAJIMA, K., MATSUSHITA, M., MAKI, H., IGARASHI, K., DAI, Z., WHITE, P. J., MCGARRAH, R. W., ILKAYEVA, O. R., DELEYE, Y., OGURI, Y., KURODA, M., IKEDA, K., LI, H., UENO, A., OHISHI, M., ISHIKAWA, T., KIM, K., CHEN, Y., SPONTON, C. H., PRADHAN, R. N., MAJD, H., GREINER, V. J., YONESHIRO, M., BROWN, Z., CHONDRONIKOLA, M., TAKAHASHI, H., GOTO, T., KAWADA, T., SIDOSSIS, L., SZOKA, F. C., MCMANUS, M. T., SAITO, M., SOGA, T. & KAJIMURA, S. 2019. BCAA catabolism in brown fat controls energy homeostasis through SLC25A44. *Nature,* 572**,** 614-619.

YU, D., RICHARDSON, N. E., GREEN, C. L., SPICER, A. B., MURPHY, M. E., FLORES, V., JANG, C., KASZA, I., NIKODEMOVA, M., WAKAI, M. H., TOMASIEWICZ, J. L., YANG, S. E., MILLER, B. R., PAK, H. H., BRINKMAN, J. A., ROJAS, J. M., QUINN, W. J., 3RD, CHENG, E. P., KONON, E. N., HAIDER, L. R., FINKE, M., SONSALLA, M., ALEXANDER, C. M., RABINOWITZ, J. D., BAUR, J. A., MALECKI, K. C. & LAMMING, D. W. 2021a. The adverse metabolic effects of branched-chain amino acids are mediated by isoleucine and valine. *Cell Metab,* 33**,** 905-922.e6.

YU, S., MENG, S., XIANG, M. & MA, H. 2021b. Phosphoenolpyruvate carboxykinase in cell metabolism: Roles and mechanisms beyond gluconeogenesis. *Mol Metab,* 53**,** 101257.

ZHANG, S., HULVER, M. W., MCMILLAN, R. P., CLINE, M. A. & GILBERT, E. R. 2014. The pivotal role of pyruvate dehydrogenase kinases in metabolic flexibility. *Nutr Metab (Lond),* 11**,** 10.

ZHANG, X. Y., GUO, C. C., YU, Y. X., XIE, L. & CHANG, C. Q. 2020. [Establishment of high-fat diet-induced obesity and insulin resistance model in rats]. *Beijing Da Xue Xue Bao Yi Xue Ban,* 52**,** 557-563.

ZHANG, Y., GUO, K., LEBLANC, R. E., LOH, D., SCHWARTZ, G. J. & YU, Y. H. 2007. Increasing dietary leucine intake reduces diet-induced obesity and improves glucose and cholesterol metabolism in mice via multimechanisms. *Diabetes,* 56**,** 1647-54.

ZHOU, M., SHAO, J., WU, C. Y., SHU, L., DONG, W., LIU, Y., CHEN, M., WYNN, R. M., WANG, J., WANG, J., GUI, W. J., QI, X., LUSIS, A. J., LI, Z., WANG, W., NING, G., YANG, X., CHUANG, D. T., WANG, Y. & SUN, H. 2019. Targeting BCAA Catabolism to Treat Obesity-Associated Insulin Resistance. *Diabetes,* 68**,** 1730-1746.

6 List of figures

7 List of tables

Acknowledgements

First and foremost, I would like to express my gratitude to Prof. Dr. Hadi Al-Hasani for the opportunity to be part of GRK 2676 VIVID and to realize this project at his institute, as well as for his constant support. I also extend my thanks to Prof. Dr. Maria Grandoch for taking on the role of co-supervisor and for her support.

I am especially grateful to Dr. Alexandra Chadt for her supervision, support, and professional expertise. She was always there for me and my project, finding time for me despite her numerous commitments, and providing great support in every respect.

I also thank Anna Scheel for her support as the supervising doctoral candidate and the entire research group, who were always there to advise and assist me with any questions. The time spent together was very enriching, and I have learned a great deal for my life through you all.

A heartfelt thank you also goes to my friends. Your unwavering support and encouraging words have been a constant source of motivation for me.

With all my heart, I thank my family for their unconditional support. You were always there for me, strengthening me through the highs and lows of this journey and my studies. Without you, none of this would have been possible. Thank you.